nature immunology

Article

https://doi.org/10.1038/s41590-022-01326-8

SUSD2 suppresses CD8$^+$ T cell antitumor immunity by targeting IL-2 receptor signaling

Received: 2 December 2021

Accepted: 8 September 2022

Published online: 20 October 2022

Check for updates

Bao Zhao[1,2], Weipeng Gong[1], Anjun Ma[3], Jianwen Chen[1], Maria Velegraki[2], Hong Dong[1], Zihao Liu[1], Lingling Wang[2,4], Tamio Okimoto[2,5], Devin M. Jones[1], Yu L. Lei[6], Meixiao Long[2,4], Kenneth J. Oestreich[1], Qin Ma[2,3], Gang Xin[1,2], David P. Carbone[2,5], Kai He[2,5], Zihai Li[2] and Haitao Wen[1,2]

Dysfunctional CD8$^+$ T cells, which have defective production of antitumor effectors, represent a major mediator of immunosuppression in the tumor microenvironment. Here, we show that SUSD2 is a negative regulator of CD8$^+$ T cell antitumor function. *Susd2*$^{-/-}$ effector CD8$^+$ T cells showed enhanced production of antitumor molecules, which consequently blunted tumor growth in multiple syngeneic mouse tumor models. Through a quantitative mass spectrometry assay, we found that SUSD2 interacted with interleukin (IL)-2 receptor α through sushi domain-dependent protein interactions and that this interaction suppressed the binding of IL-2, an essential cytokine for the effector functions of CD8$^+$ T cells, to IL-2 receptor α. SUSD2 was not expressed on regulatory CD4$^+$ T cells and did not affect the inhibitory function of these cells. Adoptive transfer of *Susd2*$^{-/-}$ chimeric antigen receptor T cells induced a robust antitumor response in mice, highlighting the potential of SUSD2 as an immunotherapy target for cancer.

Despite the recent development of immune checkpoint blockade (ICB) as a revolutionizing cancer treatment, only a small fraction of patients gain sustained clinical benefit from this therapy[1]. The decline of immune function in effector CD8$^+$ T cells, a key feature of immunosuppressive tumor microenvironment (TME) in patients with cancer who show resistance to ICB[2,3], is largely responsible for the failure to achieve durable clinical response. The existence of multiple immune checkpoint molecules means that individual targeting of single molecules cannot override the compensatory signals from the other inhibitory receptors[4,5] and there is an urgent need to identify new target(s) to rejuvenate CD8$^+$ T cell antitumor immunity, either alone or in combination with existing ICB treatments.

The growth factor IL-2 drives the expansion of activated human T cells[6] and regulates the effector and memory responses of mouse and human CD8$^+$ T cells[7,8]. The high-affinity IL-2 receptor (IL-2R) is a heterotrimeric complex composed of IL-2Rα, IL-2Rβ and the common γ chain[9–11]. IL-2Rα contains two sushi domains (SDs), which are required for IL-2 binding with IL-2Rα[12]. IL-2Rα is required for the expansion and functions of effector and memory CD8$^+$ T cells, but not in the priming of naive CD8$^+$ T cells[13–15]. In addition, the lack of IL-2 signaling leads to dysregulated T cell activation and autoimmunity, due to the essential role of IL-2 in the generation and maintenance of CD4$^+$ regulatory T (T_{reg}) cells[16]. As such, the therapeutic potential of IL-2 on CD8$^+$ T cell-mediated immunotherapy has been counteracted by the suppressive effect of T_{reg} cells on antitumor immunity[17]. Enhancement of IL-2 signaling selectively on CD8$^+$ T cells, but not T_{reg} cells, may facilitate the antitumor response of CD8$^+$ T cells.

SUSD2 is a single-pass type 1 membrane protein with an SD located on its C terminus[18]. SDs are based on a β-sandwich structure and mediate protein–protein interactions[19]. Expression of SUSD2 has been reported in a variety of human cancers, such as breast, ovarian, non-small cell lung, gastric and colorectal cancer[20–26]. Expression of SUSD2 in cancer

[1]Department of Microbial Infection and Immunity, Infectious Disease Institute, The Ohio State University, Columbus, OH, USA. [2]Pelotonia Institute for Immuno-Oncology, The Ohio State University, Comprehensive Cancer Center, The Ohio State University, Columbus, OH, USA. [3]Department of Biomedical Informatics, The Ohio State University, Columbus, OH, USA. [4]Department of Internal Medicine, Division of Hematology, The Ohio State University, Columbus, OH, USA. [5]Department of Internal Medicine, Division of Medical Oncology, The Ohio State University, Columbus, OH, USA. [6]Department of Periodontics and Oral Medicine, University of Michigan School of Dentistry, Ann Arbor, MI, USA. e-mail: Haitao.Wen@osumc.edu

cells correlates either positively or negatively with tumor growth, depending on the cancer type[20–26], but the role of SUSD2 in the antitumor immunity remains unknown. Here, we found an inhibitory effect of SUSD2 on the antitumor function of CD8$^+$ T cell by modulating IL-2Rα signaling. SUSD2 was selectively expressed in effector CD8$^+$ T cells, but not in CD4$^+$ T_{reg} cells, and uniquely inhibited CD8$^+$ T cells.

Results

Antitumor immune responses are improved in *Susd2*$^{-/-}$ mice

Gene profiling assays found that high expression of SUSD2 correlated with tumor growth in an experimental colitis-associated colorectal cancer model[27]. *Susd2*$^{-/-}$ mice generated on a C57BL/6 genetic background by deleting all 15 exons of the *Susd2* gene (Extended Data Fig. 1a,b) had no apparent defects in growth and development, including fertility, breeding, body weight or behavior (data not shown). Analyses of the adaptive and innate immune system found no alteration in the number of NK1.1$^+$ natural killer (NK) cells, CD3$^+$CD4$^+$ and CD3$^+$CD8$^+$ T cells, CD19$^+$ B cells, CD4$^+$CD25$^+$ T_{reg} cells, CD11b$^+$F4/80$^+$ macrophages, CD11b$^+$CD11c$^+$ conventional dendritic cells (DCs), CD11b$^+$Ly6C$^+$ monocytes or CD11b$^+$Ly6G$^+$ neutrophils in the spleens of naive *Susd2*$^{-/-}$ mice (Extended Data Fig. 1c–j), suggesting no change in global immune cell populations at steady state. In multiple syngeneic mouse tumor models, including allografts of MC38 colorectal cancer (Fig. 1a), EG7 thymoma (Fig. 1b) and ovalbumin-expressing B16 (B16-OVA) melanoma (Fig. 1c) in the right flanks, tumor growth was significantly blunted in *Susd2*$^{-/-}$ mice compared to wild-type C57BL/6 mice. These observations indicated that loss of SUSD2 inhibited syngeneic tumor growth.

To examine the immune profiles in the TME, we performed single-cell RNA sequencing (scRNA-seq) in CD45$^+$ immune cells isolated from MC38 tumors in wild-type and *Susd2*$^{-/-}$ mice at day 18 after inoculation. Unsupervised clustering identified 18 distinctive clusters that represented various immune cell populations, including macrophages, DCs, neutrophils, NK cells, T cells and B cells (Fig. 1d and Supplementary Table 1). Among the five clusters representing CD8$^+$ cells (clusters 3–7), we found opposite changes between cluster 3 and cluster 6 in *Susd2*$^{-/-}$ mice compared to wild-type mice (Fig. 1e), indicating that SUSD2 might affect the differentiation of intratumoral CD8$^+$ T cell subsets. Sub-clustering of CD8$^+$ T cells indicated a substantial increase in *Ifng*$^+$*Gzmb*$^+$*Cx3cr1*$^+$ effector-like T cells (CD8$^+$ T_{eff} cells, cluster 2) and a decrease in *Tcf7*$^-$*Pdcd1*$^+$*Havcr2*$^+$*Lag3*$^+$ terminally exhausted T cells (CD8$^+$ T_{ExT} cells, cluster 3) in tumors from *Susd2*$^{-/-}$ mice compared to those from wild-type mice (Fig. 1f,g and Supplementary Table 2)[28–32]. We also detected decreased *Tcf7*$^+$*Pdcd1*$^-$*Havcr2*$^-$ naive T cells (CD8$^+$ T_N cells, cluster 0) and slightly increased *Tcf7*$^+$*Pdcd1*$^+$*Havcr2*$^-$*Lag3*$^-$ progenitor exhausted T cells (CD8$^+$ T_{ExP} cells, cluster 1) in tumors from *Susd2*$^{-/-}$ mice compared to those from wild-type mice (Fig. 1f,g). Further examination of gene signature in CD8$^+$ cells indicated increased expression of various genes encoding T cell effector molecules, such as *Gzmb* and *Ifng* in *Susd2*$^{-/-}$ CD8$^+$ cells compared to wild-type CD8$^+$ cells (Fig. 1h,i). Pathway enrichment analysis discovered higher expression of genes involved in multiple antitumor immunity-related pathways, such as cytokine–cytokine receptor interaction, in *Susd2*$^{-/-}$ CD8$^+$ cells compared to wild-type CD8$^+$ T cells (Fig. 1j). These findings suggested that SUSD2 deficiency led to an enhanced differentiation of CD8$^+$ T_{eff} cells and reduced transition to CD8$^+$ T_{ExT} cells in the TME, which correlate with an improved control of tumor growth.

Flow cytometry analysis of MC38 tumors at day 18 after inoculation indicated the frequencies of immune cells, including CD11b$^+$F4/80$^+$ macrophages, CD11b$^+$CD11c$^+$ DCs, CD11b$^+$Ly6C$^+$ monocytes, CD11b$^+$Ly6G$^+$ neutrophils and NK1.1$^+$ NK cells, among the CD45$^+$ tumor-infiltrating leukocytes were similar between wild-type and *Susd2*$^{-/-}$ mice (Extended Data Fig. 2a–e). In contrast, a significantly increased percentage of CD8$^+$ T cells (20% versus 14% of CD45$^+$ cells), but not CD4$^+$ T cells or Foxp3$^+$ T_{reg} cells, were detected in M38 tumors in *Susd2*$^{-/-}$ compared to wild-type C57BL/6 mice (Fig. 2a,b). The production of interferon (IFN)-γ, GzmB and tumor necrosis factor (TNF) was significantly enhanced in intratumoral CD8$^+$ T cells from *Susd2*$^{-/-}$ mice compared to wild-type mice (Fig. 2c), whereas intratumoral NK cells generated similar amounts of IFN-γ and CD4$^+$ T cells generated similar amounts of IFN-γ, GzmB and TNF in *Susd2*$^{-/-}$ mice and wild-type mice (Extended Data Fig. 2f,g), indicating an elevated antitumor immune response uniquely in *Susd2*$^{-/-}$ CD8$^+$ T cells. Enhanced production of IFN-γ, GzmB and TNF in intratumoral *Susd2*$^{-/-}$ CD8$^+$ T cells compared to wild-type CD8$^+$ T cells was also observed in mice challenged with EG7 or B16-OVA cells (Fig. 2d,e).

Multi-dimensional flow cytometry assay with a panel of 32 lineage- and T cell state-specific markers indicated that *Susd2*$^{-/-}$ CD8$^+$ T cells localized substantially more in subcluster 1 and subcluster 2, which were defined as CD8$^+$ T_{eff} cells based on the enriched expression of IFN-γ, TNF, CXCR3 and KLRG1, and less in subclusters 12, 13, 14 and 19, which were defined as CD8$^+$ T_{ExT} cells, based on the high expression of Tim-3, TOX, Lag3, CD38 and CD39, compared to wild-type CD8$^+$ T cells (Fig. 2f–h and Extended Data Fig. 2h,i). *Susd2*$^{-/-}$ CD8$^+$ T cells were also significantly increased in subcluster 7, which was defined as TCF1^{hi}PD-1$^+$Tim-3$^-$CD8$^+$ T_{ExP} cells (Fig. 2g,h). Depletion of CD8$^+$ T cells completely abolished the improved control of MC38 tumor growth in *Susd2*$^{-/-}$ mice compared to wild-type mice (Fig. 2i), suggesting that enhanced CD8$^+$ T_{eff} cell function was a key contributor to the control of tumor growth in *Susd2*$^{-/-}$ mice.

Next, we asked whether *Susd2*$^{-/-}$ CD8$^+$ T cells exhibited altered expression of immune checkpoint molecules[4,5]. Expression of PD-1 and LAG3 (refs. [4,28]) was similar in intratumoral wild-type and *Susd2*$^{-/-}$ CD8$^+$ T cells in mice challenged with MC38, EG7 or B16-OVA cells (Extended Data Fig. 2j–l). MC38 tumor growth was significantly delayed in *Susd2*$^{-/-}$ mice treated with PD-L1 antibody compared to similarly treated wild-type mice (Fig. 2j), which translated into extended survival (Fig. 2j). Despite tumor growth showing minimal response to PD-L1 antibody treatment in wild-type mice[33], tumor growth was significantly attenuated and survival was improved in PD-L1 antibody-treated *Susd2*$^{-/-}$ mice challenged with either EG7 (Fig. 2k) or B16-F10 (Fig. 2l) cells. Moreover, MC38 tumors exhibited a significantly delayed growth, alongside increased survival in *Susd2*$^{-/-}$ mice compared to wild-type mice treated with PD-1 antibody (Fig. 2m). In sum, deletion of *Susd2* synergized with PD-1 and PD-L1 blockade treatments to improve antitumor immunity.

Susd2$^{-/-}$CD8$^+$ T cells show enhanced antitumor function

Next, we examined whether SUSD2 directly modulated CD8$^+$ T cell function. In various immune cell populations sorted from the spleen

Fig. 1 | Genetic deletion of *Susd2* results in improved antitumor immunity. **a**–**c**, Tumor growth at 7, 9, 11, 13, 15, 17, 19 and 21 d after inoculation with MC38 (**a**), EG7 (**b**) or B16-OVA (**c**) tumor cells in wild-type (WT) and *Susd2*$^{-/-}$ mice. Dotted lines show values from an individual mouse; solid lines represent mean values. **d**,**e**, Uniform Manifold Approximation and Projection (UMAP) of intratumoral CD45$^+$ cells (**d**) and quantitation of each cell type (**e**) in WT and *Susd2*$^{-/-}$ mice 18 d after inoculation with MC38 tumors. Clusters denoted by color are labeled with inferred cell types (**d**). MDSC (*Itgam*, *Arg1*, *Pf4*); MoDC (*Ccr2*, *H2-DMa*, *H2-Ab1*); pDC (*Siglech*, *Bst2*). **f**,**g**, UMAP (**f**) and quantitation (**g**) of intratumoral *Cd8a*$^+$*Trbc1*$^+$*Trbc2*$^+$ cells in WT and *Susd2*$^{-/-}$ mice 18 d after inoculation with MC38 tumors. Clusters are labeled with inferred intratumoral CD8$^+$ cell subtypes (**f**). **h**,**i**, Heat map of differentially expressed genes between WT and *Susd2*$^{-/-}$ intratumoral CD8$^+$ cells (**h**) and violin plots showing *Ifng* and *Gzmb* expression in WT and *Susd2*$^{-/-}$ intratumoral CD8$^+$ cells (**i**) from mice as in **d**,**e**. **j**, Gene Ontology enrichment in WT and *Susd2*$^{-/-}$ intratumoral CD8$^+$ cells from mice as in **d**,**e**. Hypergeometric test was used for functional enrichment in Enrichr. All *P* values were Benjamini–Hochberg adjusted for multiple comparisons. $n = 10$ (**a**); $n = 7$ (**b**); WT, $n = 6$ (**c**); *Susd2*$^{-/-}$ $n = 7$. Data are representative of four independent experiments (**a**–**c**) and two independent experiments (**d**–**j**). Statistical significance was calculated with two-way analysis of variance (ANOVA) followed by Tukey's multiple comparisons test with *P* values noted in **a**–**c**.

https://doi.org/10.1038/s41590-022-01326-8

of naive C57BL/6 mice, CD8$^+$ T cells had the highest amount of *Susd2* transcript (Fig. 3a). Highest amounts of SUSD2 mRNA and protein were also detected in human CD8$^+$ T cells isolated from peripheral blood mononuclear cells (PBMCs) (Fig. 3b,c). Stimulation with CD3-CD28 antibodies induced a marked increase in the amount of *Susd2* transcript in sorted mouse CD8$^+$ T cells, whereas mouse CD4$^+$ T cells exhibited a

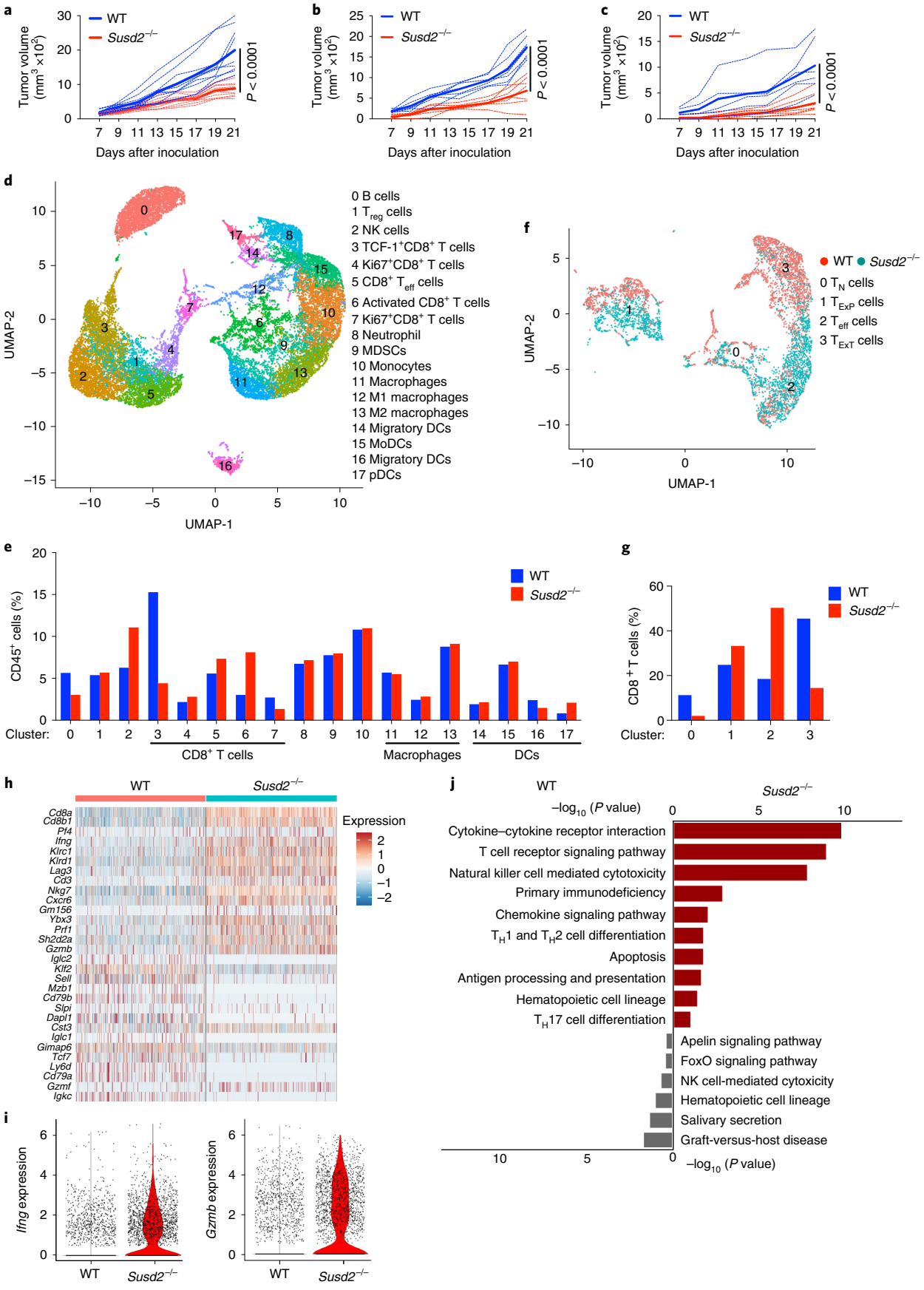

https://doi.org/10.1038/s41590-022-01326-8

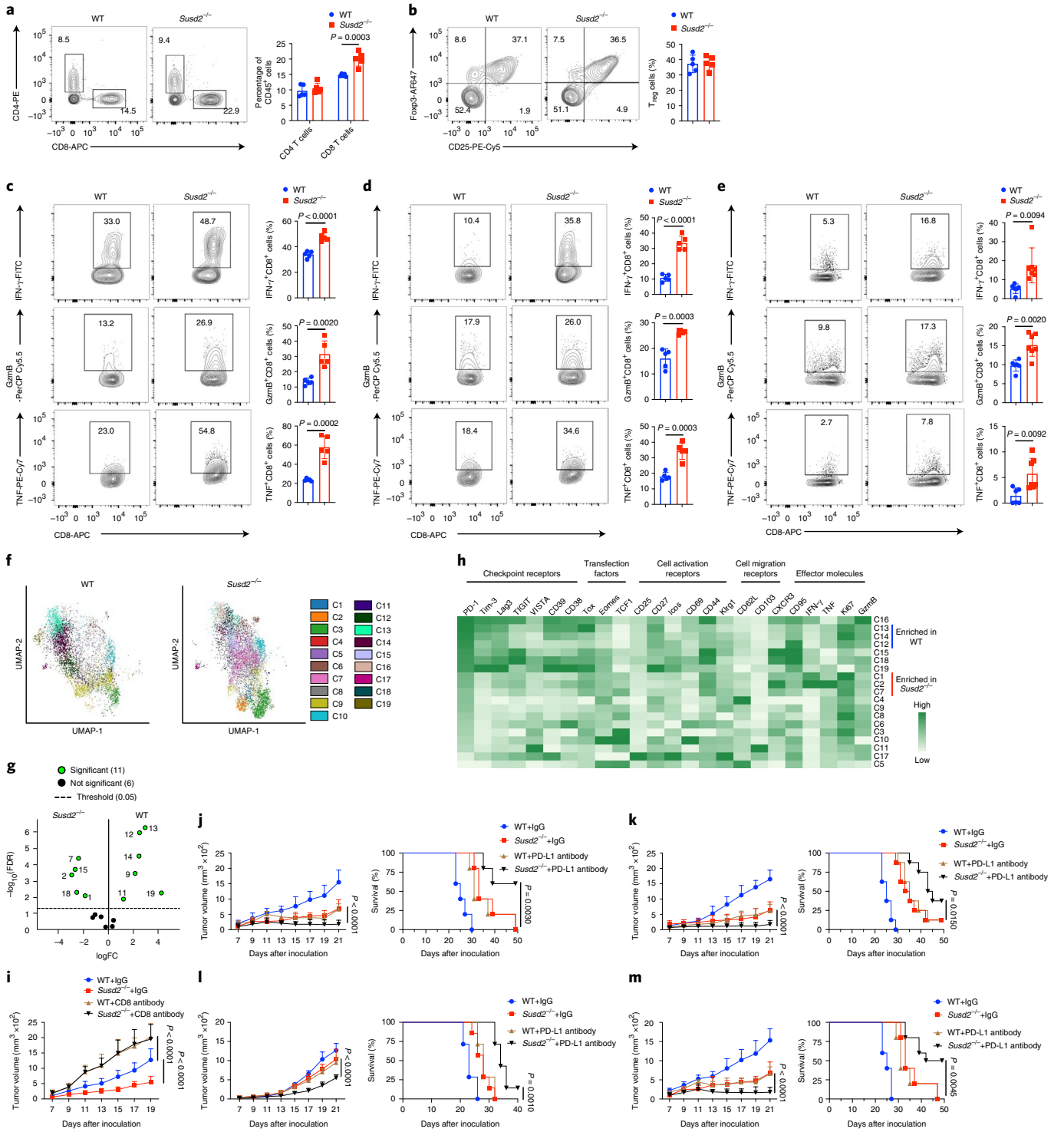

Fig. 2 | Enhanced antitumor response in *Susd2*$^{-/-}$ mice depends on CD8$^+$ cells. a,**b**, Flow cytometry analysis showing percentage of CD4$^+$ and CD8$^+$ T cells (**a**) and CD25$^+$Foxp3$^+$ T_{reg} cells (**b**) in MC38 subcutaneous tumor isolated from WT or *Susd2*$^{-/-}$ mice 18 d after tumor inoculation (**a**,**b**). **c**–**e**, Flow cytometry analysis showing intracellular accumulation of IFN-γ, GzmB and TNF-expressing intratumoral CD8$^+$ T cells in MC38 (**c**), EG7 (**d**) or B16-OVA (**e**) tumors isolated from WT or *Susd2*$^{-/-}$ mice 18 d after tumor inoculation. **f**–**h**, UMAP analysis (**f**), volcano plot illustrating differential abundance clusters (**g**) and cluster-by-marker heat map characterizing the expression patterns of individual clusters (**h**) of intratumoral CD8$^+$ T cells from WT and *Susd2*$^{-/-}$ mice 18 d after inoculation with MC38. **i**, Tumor growth in MC38 tumor-bearing WT or *Susd2*$^{-/-}$ mice injected with either control IgG or CD8 antibody at 0, 7 and 14 d after tumor inoculation. **j**–**l**, Tumor growth and survival in WT and *Susd2*$^{-/-}$ mice bearing either MC38 (**j**), EG7 (**k**) or B16-F10 (**l**) tumor cells injected with either control IgG or PD-L1 antibody at 7, 10 and 13 d after tumor inoculation. **m**, Tumor growth and survival in WT and *Susd2*$^{-/-}$ mice inoculated with MC38 tumor cells and injected with control IgG or PD-1 antibody at 7, 10 and 13 d after tumor inoculation. $n = 5$ mice per group (**a**–**d**,**i**,); WT, $n = 6$, *Susd2*$^{-/-}$, $n = 7$ (**e**); $n = 8$ (**f**–**h**,**k**); $n = 7$ (**l**); and $n = 10$ (**j**,**m**). Data are representative of three independent experiments (**a**–**e**,**i**-**m**) and two independent experiments (**f**–**h**). Statistical significance was determined by two-tailed unpaired Student's *t*-test (**a**–**e**). *P* values were calculated using two-sided Wilcoxon's rank-sum test and adjusted with Bonferroni's correction (**g**), two-way ANOVA followed by Tukey's multiple comparisons test (**i**,**j** left, **k** left, **l** left, **m** left) or log-rank (Mantel–Cox) test survival analysis (**j** right, **k** right, **l** right, **m** right) with *P* values noted in the figure. Data represent mean ± s.d.

moderate increase 3 d after stimulation (Fig. 3d,e). SUSD2 mRNA and protein were also augmented in human $CD8^+$ T cells by stimulation with CD3-CD28 antibodies (Fig. 3f,g). Increased *Susd2* mRNA expression was detected in $CD8^+$ T cells, but not $CD4^+$ T cells, infiltrating the MC38 tumors compared to splenic $CD8^+$ T cells (Fig. 3h). Therefore, SUSD2 was highly expressed in mouse and human $CD8^+$ T cells and its expression was further upregulated by T cell antigen receptor activation.

Next, we challenged total splenocytes from *Susd2*$^{-/-}$ OT-I mice with the cognate antigen peptide $OVA_{257-264}$. *Susd2*$^{-/-}$$CD8^+$ OT-I T cells generated significantly higher amounts of IFN-γ, GzmB and TNF (Fig. 3i–k and Extended Data Fig. 3a), as well as significantly attenuated cell apoptosis, as assayed by staining with 7-AAD and annexin V, after antigen stimulation for 3 d (Fig. 3l), compared to wild-type $CD8^+$ OT-I T cells. RNA-seq in splenic $CD8^+$ T cells isolated from wild-type or *Susd2*$^{-/-}$ OT-I mice stimulated or not with $OVA_{257-264}$ for 3 d (Extended Data Fig. 3b–e and Supplementary Tables 3 and 4) detected elevated expression of genes encoding T cell effector molecules, including *Ifng*, *Prf1*, *Tnfa*, *Gzmc*, in $OVA_{257-264}$-activated *Susd2*$^{-/-}$ compared to wild-type $CD8^+$ OT-I T cells (Extended Data Fig. 3d,e and Supplementary Table 4). *Susd2*$^{-/-}$$CD8^+$ OT-I T cells also exhibited enhanced cytotoxicity toward OVA peptide-pulsed MC38, EG7 or B16-OVA cells compared to wild-type $CD8^+$ OT-I T cells (Fig. 3m). In an antigen-presenting assay, wild-type or *Susd2*$^{-/-}$ bone marrow-derived dendritic cells (BMDCs) pulsed with $OVA_{257-264}$ were cultured with $CD8^+$ T cells isolated from wild-type or *Susd2*$^{-/-}$ OT-I mice[34]. *Susd2*$^{-/-}$$CD8^+$ T cells generated significantly higher amounts of IFN-γ, regardless of the BMDC genotypes, compared to wild-type $CD8^+$ T cells (Extended Data Fig. 3f), suggesting the inhibitory effect of SUSD2 was intrinsic to the $CD8^+$ T cells. Production of IFN-γ, GzmB or TNF was similar in $CD4^+$ T cells isolated from wild-type or *Susd2*$^{-/-}$ OT-II mice when total splenocytes were challenged with the cognate antigen $OVA_{323-339}$ (Extended Data Fig. 4a), while *Susd2*$^{-/-}$ T_{reg} cells expressed similar amounts of Foxp3 protein (Extended Data Fig. 4b) and had a comparable capacity to block the proliferation of naive $CD4^+$ T cells (Extended Data Fig. 4c) compared to wild-type T_{reg} cells, suggesting that loss of SUSD2 did not affect the function of $CD4^+$ T cells or T_{reg} cells.

To evaluate the antitumor function of *Susd2*$^{-/-}$ $CD8^+$ T cells in vivo, we primed Thy1.2$^+$ wild-type or *Susd2*$^{-/-}$ OT-I T cells with $OVA_{257-264}$ for 3 d and intravenously transferred them into Thy1.1$^+$ congenic wild-type mice challenged with EG7 tumor cells 7 d before cell transfer. While transfer of wild-type OT-I T cells resulted in reduced tumor growth compared to mice injected with PBS as control, transfer of *Susd2*$^{-/-}$ OT-I T cells led to complete eradication of EG7 tumor growth in all mice examined (Fig. 3n), suggesting a superior antitumor response by *Susd2*$^{-/-}$ compared to wild-type OT-I T cells. Transferred *Susd2*$^{-/-}$ OT-I T cells showed higher tumor infiltration and elevated production of IFN-γ, GzmB and TNF compared to wild-type OT-I T cells (Fig. 3o). Moreover, more intratumoral *Susd2*$^{-/-}$ OT-I T cells had a TCF1$^+$PD-1$^+$ T_{ExP} cell phenotype and a markedly decreased TCF1$^-$PD-1$^+$Tim-3$^+$ T_{EXT} cell phenotype compared to wild-type OT-I T cells (Fig. 3p,q), suggesting an attenuated transition of *Susd2*$^{-/-}$ T cells to terminal exhaustion. Collectively, these results suggested that *Susd2*$^{-/-}$$CD8^+$ T cells provided a superior antitumor effect, presumably through enhanced production of cytotoxic factors.

SUSD2–IL-2Rα interaction requires SD

Because SUSD2 contains a short (16 amino acids) undefined cytoplasmic tail, suggesting that SUSD2 may not initiate intracellular signaling directly, we investigated whether SUSD2 modulated $CD8^+$ T cell effector function through its interaction with cell surface protein(s). To determine the interactome of SUSD2 in $CD8^+$ T cells, we retrovirally transduced *Susd2*$^{-/-}$ OT-I T cells with a V5$^-$tagged mouse *Susd2* or empty vector as control, followed by V5 agarose immunoprecipitation and liquid chromatography coupled to tandem MS (LC–MS/MS). Susd2 was detected only in the precipitates from *Susd2*-reconstituted *Susd2*$^{-/-}$ OT-I T cells (Fig. 4a,b). IL-2Rα was highly enriched in the precipitates from *Susd2*-reconstituted *Susd2*$^{-/-}$ OT-I cells compared to those from *Susd2*$^{-/-}$ OT-I cells reconstituted with empty vector, based on the number of peptides (indicating the identification confidence) and the number of peptide-spectrum matches (PSMs; indicating the abundance) (Fig. 4a and Supplementary Table 5). Susd2 and IL-2Rα co-immunoprecipitated from *Susd2*-reconstituted cells activated by $OVA_{257-264}$ for 3 d (Fig. 4c), while Susd2 did not pulldown IL-2Rβ, common γ chain or IL-15Rα (Fig. 4c,d), suggesting a specific interaction between Susd2 and IL-2Rα. The authenticity of the IL-2Rα band was verified by immunoblotting of 293T cells expressing Flag-tagged IL2RA (Flag-IL2RA) (Extended Data Fig. 5a) using both human IL-2Rα (sc-365511) and Flag antibodies (Extended Data Fig. 5b). In 293T cells co-transfected with plasmids expressing V5-SUSD2 and Flag-IL2RA, SUSD2 co-immunoprecipitated with IL-2Rα (Fig. 4e,f) and colocalized with IL-2Rα on the cell surface (Fig. 4g). Overexpressed V5-SUSD2 also pulled down endogenous IL-2Rα in human Jurkat T cells (Fig. 4h), indicating that IL-2Rα interacted with SUSD2 in mouse and human cells.

Because both SUSD2 and IL-2Rα contain an SD (Fig. 4b), which is known to mediate protein–protein interaction[19], we next tested whether the interaction between SUSD2 and IL-2Rα was mediated by the SD. In 293T cells co-expressing a SUSD2 mutant protein lacking the SD ($SUSD2^{\Delta SD}$) and IL-2Rα, we could not detect an interaction between $SUSD2^{\Delta SD}$ and IL-2Rα (Fig. 4i). Deletion of SD1 in IL-2Rα resulted in the loss of SUSD2–IL-2Rα interaction, while deletion of SD2 in IL-2Rα had no effect in 293T cells co-expressing the mutant IL-2Rα proteins and $SUSD2^{WT}$ (Fig. 4j). These observations indicated that SUSD2 interacted with IL-2Rα, and the interactions was mediated by the SD in both proteins.

SUSD2 negatively regulates IL-2R signaling

Because IL-2 signaling regulates effector function of $CD8^+$ T cells[7,8,35,36], we next investigated whether SUSD2 interfered with IL-2 signaling through the IL-2R. Stimulation of naive $CD8^+$ T cells with the γ chain family cytokine IL-2, IL-7 or IL-15 only induced a slight increase in the expression of *Susd2*, in contrast to the strong upregulation of *Susd2* gene transcription in T cell antigen receptor-activated $CD8^+$ T cells (Extended Data Fig. 6a). When $OVA_{257-264}$-activated OT-I T cells were rested overnight before stimulation with either IL-2, IL-7 or IL-15 (ref. [7]), IL-2-treated *Susd2*$^{-/-}$ OT-I T cells showed enhanced phosphorylation of STAT5, an essential transcription factor downstream of IL-2 signaling[36], and elevated production of GzmB compared to IL-2-treated wild-type OT-I T cells (Fig. 5a,b and Extended Data Fig. 6b), whereas IL-7- or IL-15-treated wild-type and *Susd2*$^{-/-}$ OT-I T cells induced the same amount of p-STAT5 and GzmB (Fig. 5a,b and Extended Data Fig. 6c,d). p-STAT5 was comparable in IL-2-treated wild-type and *Susd2*$^{-/-}$ T_{reg} cells (Extended Data Fig. 6e), suggesting that SUSD2 specifically affected IL-2R signaling in $CD8^+$ T cells. Blocking antibodies for IL-2 (clone JES6-1A12)[13] or IL-2Rα (clone PC61), but not blocking antibodies for IL-2Rβ (clone TM-β1), abolished the elevated production of IFN-γ and GzmB in *Susd2*$^{-/-}$ OT-I T cells stimulated with a suboptimal dose (200 ng ml^{-1}) of $OVA_{257-264}$ (Fig. 5c,d). The enhanced production of IFN-γ (Extended Data Fig. 6f) and increased apoptosis (Fig. 5e) of *Susd2*$^{-/-}$ $CD8^+$ T cells co-cultured with $OVA_{257-264}$-pulsed were attenuated by blocking antibodies against IL-2 or IL-2Rα, but not IL-2Rβ. Cell surface expression of IL-2Rα was similar between wild-type and *Susd2*$^{-/-}$ OT-I T cells (Fig. 5f), indicating that enhanced IL-2 signaling in *Susd2*$^{-/-}$ OT-I T cells was not due to elevated expression of IL-2Rα.

Based on the crystal structure of IL-2 in complex with IL-2Rα, IL-2 engages IL-2Rα along the length of SD1 (ref. [12]). To test the hypothesis that SUSD2 competitively blocked the SD-dependent binding of IL-2 to IL-2Rα, we performed an IL-2 binding assay using biotinylated IL-2 in 293T cells that overexpressed V5–SUSD2 and/or Flag–IL2RA. We did not detect direct binding between SUSD2 and biotinylated IL-2, but overexpression of V5–SUSD2 significantly decreased binding of biotinylated IL-2 to overexpressed Flag–IL2RA (Fig. 5g). Increased

https://doi.org/10.1038/s41590-022-01326-8

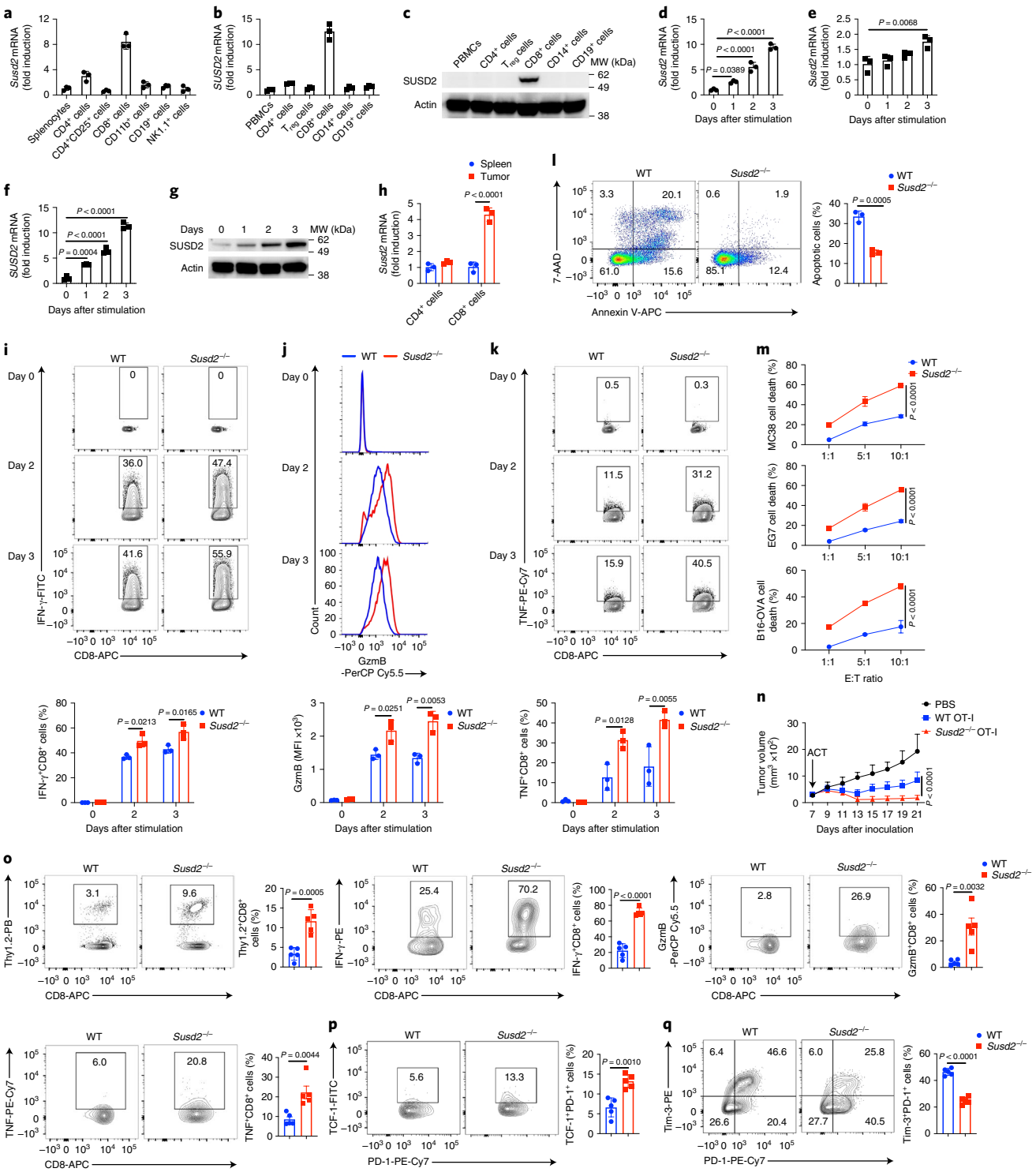

Fig. 3 | *Susd2*$^{-/-}$ CD8$^+$ cells exhibit increased antitumor effector function and survival. a–**c**, Transcript (**a**,**b**) and protein (**c**) of *SUSD2* in various immune cell types isolated from mouse spleen (**a**) or human PBMCs (**b**,**c**). **d**–**g**, Transcript (**d**–**f**) and protein (**g**) of *SUSD2* in sorted mouse CD8$^+$ T cells, mouse CD4$^+$ T cells and human CD8$^+$ T cells that have been left untreated or stimulated with CD3-CD28 antibodies. **h**, Expression of *Susd2* transcript in CD4$^+$ and CD8$^+$ T cells isolated from either spleen or tumor tissue in mice bearing MC38 tumor. **i**–**k**, Representative flow cytometry analysis showing IFN-γ$^+$CD8$^+$ T cells, GzmB$^+$CD8$^+$ T cells and TNF$^+$CD8$^+$ T cells in OVA$_{257-264}$ stimulated splenocytes isolated from WT or *Susd2*$^{-/-}$ OT-I mice at day 0, 2 and 3. **l**, Flow cytometry analysis showing annexin V$^+$7-AAD$^+$CD8$^+$ T cells in OVA$_{257-264}$-stimulated splenocytes isolated from WT or *Susd2*$^{-/-}$ OT-I mice at day 3. **m**, In vitro killing of OVA$_{257-264}$ peptide-pulsed MC38 (top), EG7 (middle) and B16-OVA (bottom) cells by WT or *Susd2*$^{-/-}$ OT-I T cells after co-culture for 4 h. **n**, Tumor growth in EG7-bearing mice after transfer with PBS, OVA$_{257-264}$ primed WT or *Susd2*$^{-/-}$ OT-I T cells. **o**–**q**, Flow cytometry analysis showing Thy1.2$^+$CD8$^+$ T cells, IFN-γ$^+$CD8$^+$ T cells, GzmB$^+$CD8$^+$ T cells, TNF$^+$CD8$^+$ T cells, TCF-1$^+$PD-1$^+$CD8$^+$ T cells and Tim-3$^+$PD-1$^+$CD8$^+$ T cells in EG7 isolated from OVA$_{257-264}$ primed WT or *Susd2*$^{-/-}$ OT-I T cells transferred tumor-bearing mice at 18 d after tumor inoculation. TCF-1$^+$PD-1$^+$CD8$^+$ T cells were gated from PD-1$^+$CD8$^+$ T cells. $n = 3$ mice per group (**a**,**b**,**d**–**f**,**h**–**m**); $n = 5$ mice per group (**n**–**q**). Data are representative of three independent experiments (**a**–**h**,**n**–**q**) and four independent experiments (**i**–**m**). Statistical significance was determined by one-way ANOVA followed by Tukey's test (**a**,**b**,**d**–**f**), two-tailed unpaired Student's *t*-test (**l**,**o**–**q**) or two-way ANOVA followed by Sidak's multiple comparisons test (**h**–**k**,**m**) or Tukey's multiple comparisons test (**n**) with *P* values noted in the figure. Data represent mean ± s.d.

https://doi.org/10.1038/s41590-022-01326-8

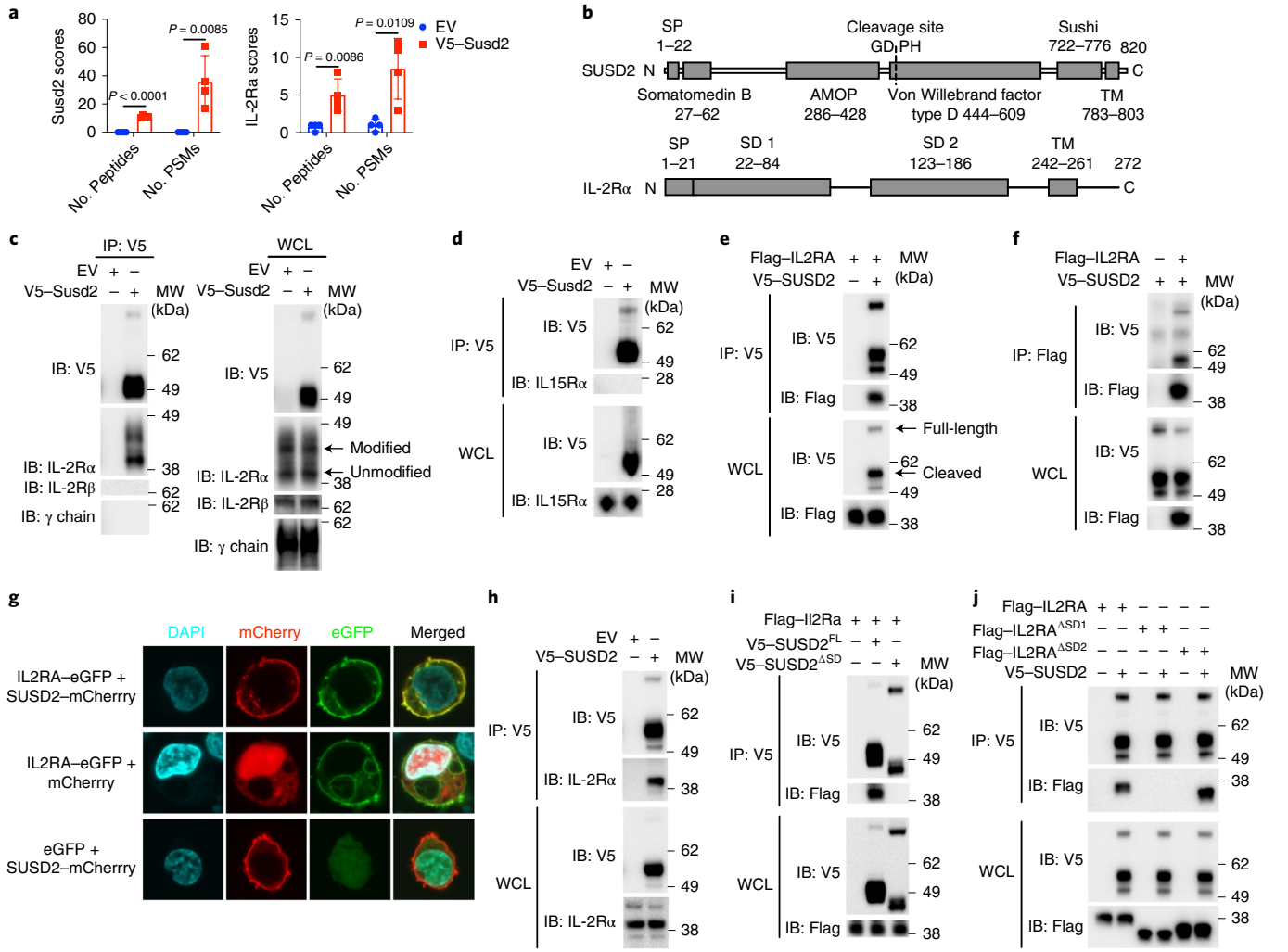

Fig. 4 | SUSD2 interacts with IL-2Rα via its sushi domain. a, LC–MS/MS of Susd2-interacting proteins in Susd2-containing protein complex immunoprecipitated from *Susd2*$^{-/-}$ OT-I T cells reconstituted with either V5-tagged mouse *Susd2* or EV. **b**, Schematic domain structure of SUSD2 and IL-2Rα. SP, signal peptide; TM, transmembrane domain. **c**,**d** Immunoblotting (IB) of IL-2Rα, IL-2Rβ or common γ chain (**c**) and IL-15Rα (**d**) in Susd2 precipitates immunoprecipitated (IP) from *Susd2*$^{-/-}$ OT-I T cells reconstituted with either EV or V5-tagged mouse *Susd2*. **e**,**f**, Immunoblot analysis of V5–SUSD2 and Flag–IL-2Rα in V5-SUSD2 or Flag–IL-2Rα precipitates immunoprecipitated from 293T cells transfected with V5–*SUSD2* and Flag–*IL2RA*. **g**, Immunofluorescence of 293T cells transfected with mCherry–SUSD2 and eGFP–IL2RA at 48 h after transfection. **h**, Immunoblot analysis of SUSD2 and IL-2Rα in V5–SUSD2 precipitates immunoprecipitated from Jurkat T cells transduced with either V5–*SUSD2* or EV. **i**, Immunoblot analysis of V5–SUSD2^{FL}, V5–SUSD2^{ΔSD} and Flag–Il-2Rα in V5–SUSD2^{FL} or V5–SUSD2^{ΔSD} precipitates immunoprecipitated from 293T cells transfected with V5–*SUSD2*^{FL}, V5–*SUSD2*^{ΔSD} and Flag–*Il2rα*. **j**, Immunoblot analysis of V5–SUSD2, Flag–IL-2Rα, Flag–IL-2Rα^{SD1} and Flag–IL-2Rα^{SD2} in V5–SUSD2 precipitates immunoprecipitated from 293T cells transfected with V5–*SUSD2*, Flag–Il2RA, Flag–*Il2RA*^{ΔSD1} and Flag–*Il2RA*^{ΔSD2}. *n* = 4 (**a**). Bars show medians and symbols show individual mice. Statistical significance was determined by two-tailed unpaired Student's *t*-test with *P* values noted in the figure. Data are from two independent experiments (**a**) and three independent experiments (**c**–**j**). Data represent mean ± s.d. WCL, whole cell lysate.

binding of biotinylated IL-2 to OVA$_{257–264}$-activated *Susd2*$^{-/-}$ OT-I T cells was observed compared to similarly treated wild-type OT-I T cells (Fig. 5h), suggesting that SUSD2 negatively regulated IL-2R signaling by interfering with IL-2–IL-2Rα binding.

Selective targeting of IL-2/IL-2 antibody immune complexes on IL-2 receptors improves IL-2 immunotherapy against tumors[13,37,38]. To examine the impact of SUSD2 on IL-2R signaling during an antitumor response in vivo, we compared the efficacy of IL-2/IL-2 antibody complexes in limiting the growth of B16-F10 tumors in wild-type and *Susd2*$^{-/-}$ mice. We used an IL-2Rα-targeting complex (IL-2/Ab$_{CD25}$, which is mouse IL-2 complexed with IL-2 antibody, clone JES6-1A12) and a CD122-targeting complex (IL-2/Ab$_{CD122}$, mouse IL-2 complexed with IL-2 antibody, clone S4B6-1)[13,37]. IL-2/Ab$_{CD25}$ had a minimal effect on tumor growth in wild-type mice compared to PBS injection, as previously reported[37] (Extended Data Fig. 6g), but significantly blunted the growth of B16-F10 tumors in *Susd2*$^{-/-}$ mice (Extended Data Fig. 6g), whereas IL-2/Ab$_{CD122}$ caused a similar reduction of tumor growth in wild-type and *Susd2*$^{-/-}$ mice (Extended Data Fig. 6h). IL-2/Ab$_{CD25}$-treated *Susd2*$^{-/-}$ mice had significantly increased percentages of intratumoral CD8$^+$ T cells that produced IFN-γ, GzmB and TNF compared to IL-2/Ab$_{CD25}$-treated wild-type mice (Extended Data Fig. 6i–k). Collectively, these findings indicated an inhibitory effect of SUSD2 on IL-2R function.

SUSD2 inhibits CD8$^+$ T cell antitumor function via SD

We next inquired whether the interaction between SUSD2 and IL-2Rα was required for the inhibitory effect of SUSD2 on CD8$^+$ T cell activation. In OVA$_{257–264}$-activated *Susd2*$^{-/-}$ OT-I T cells retrovirally transduced with green fluorescent protein (GFP)-tagged full-length SUSD2

https://doi.org/10.1038/s41590-022-01326-8

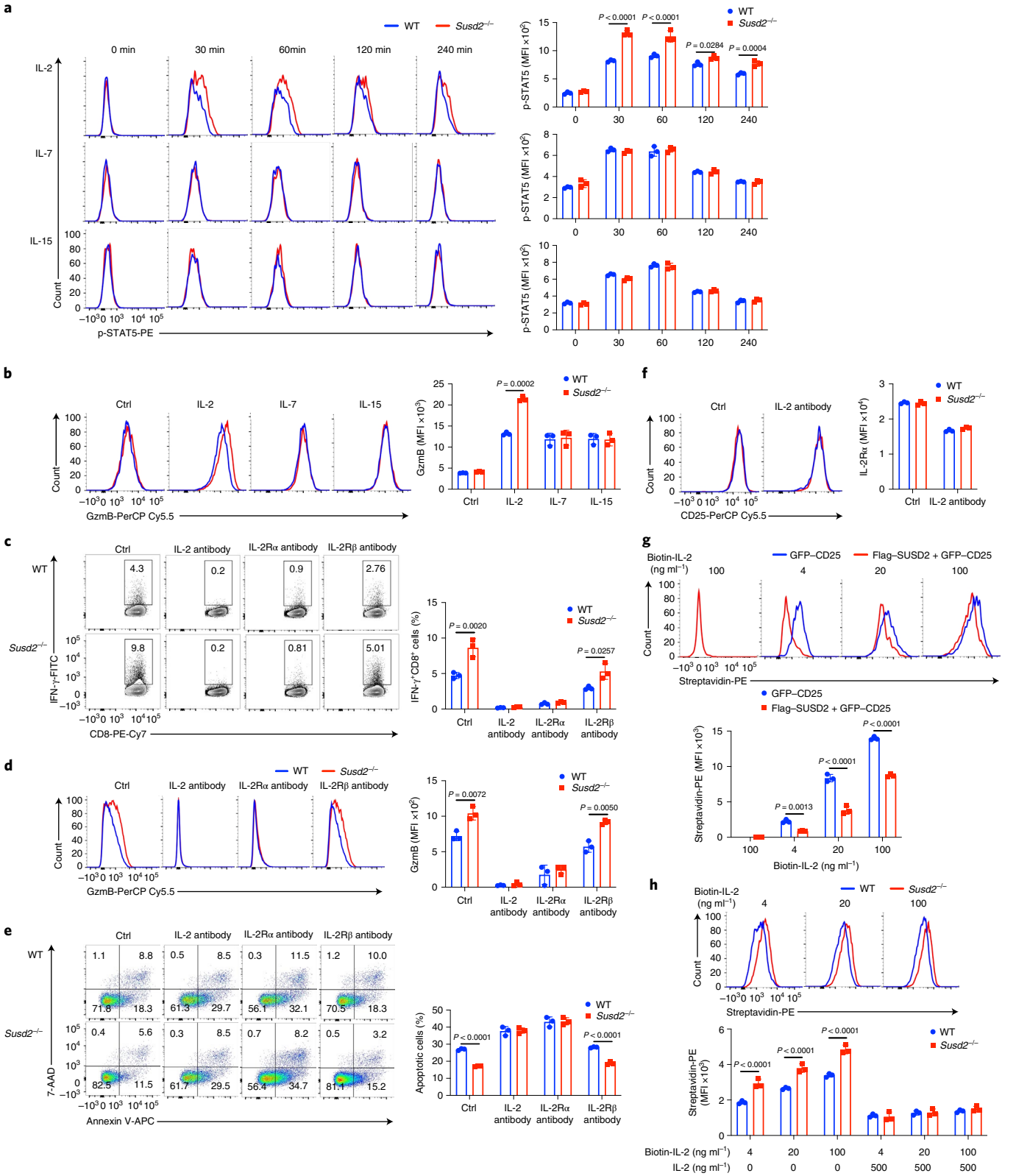

Fig. 5 | SUSD2 impairs CD8⁺ cell effector function by attenuating IL-2Rα signaling. a,**b**, Flow cytometry analysis of phosphorylated STAT5 (p-STAT5) (**a**) and intracellular GzmB (**b**) in $OVA_{257–264}$-primed WT or *Susd2*$^{-/-}$ OT-I T cells rested overnight and then stimulated with IL-2 (100 U ml^{-1}), IL-7 (5 ng ml^{-1}) or IL-15 (10 ng ml^{-1}) for 0, 30, 60, 120 and 240 min. **c**–**e**, Flow cytometry analysis of intracellular IFN-γ (**c**), GzmB (**d**) and cell apoptosis (**e**) in WT or *Susd2*$^{-/-}$ OT-I T cells stimulated with 200 ng ml^{-1} $OVA_{257–264}$ (suboptimal dose) for 48 h. **f**, Flow cytometry analysis of IL-2Rα expression in $OVA_{257–264}$-stimulated WT or *Susd2*$^{-/-}$ OT-I T cells. MFI, mean fluorescence intensity. **g**, Flow cytometry analysis of binding of biotinylated IL-2 on 293T cells overexpressing *SUSD2* and/or *IL2RA*. **h**, Flow cytometry analysis of biotinylated IL-2 binding to WT or *Susd2*$^{-/-}$ OT-I T cells treated or not with unconjugated IL-2. $n = 3$ mice per group (**a**–**h**). Data are representative of three independent experiments (**a**,**b**,**g**,**h**) and four independent experiments (**c**–**f**). Statistical significance was determined by two-way ANOVA followed by Sidak's multiple comparisons test (**a**–**h**) with *P* values noted in the figure. Data represent mean ± s.d.

https://doi.org/10.1038/s41590-022-01326-8

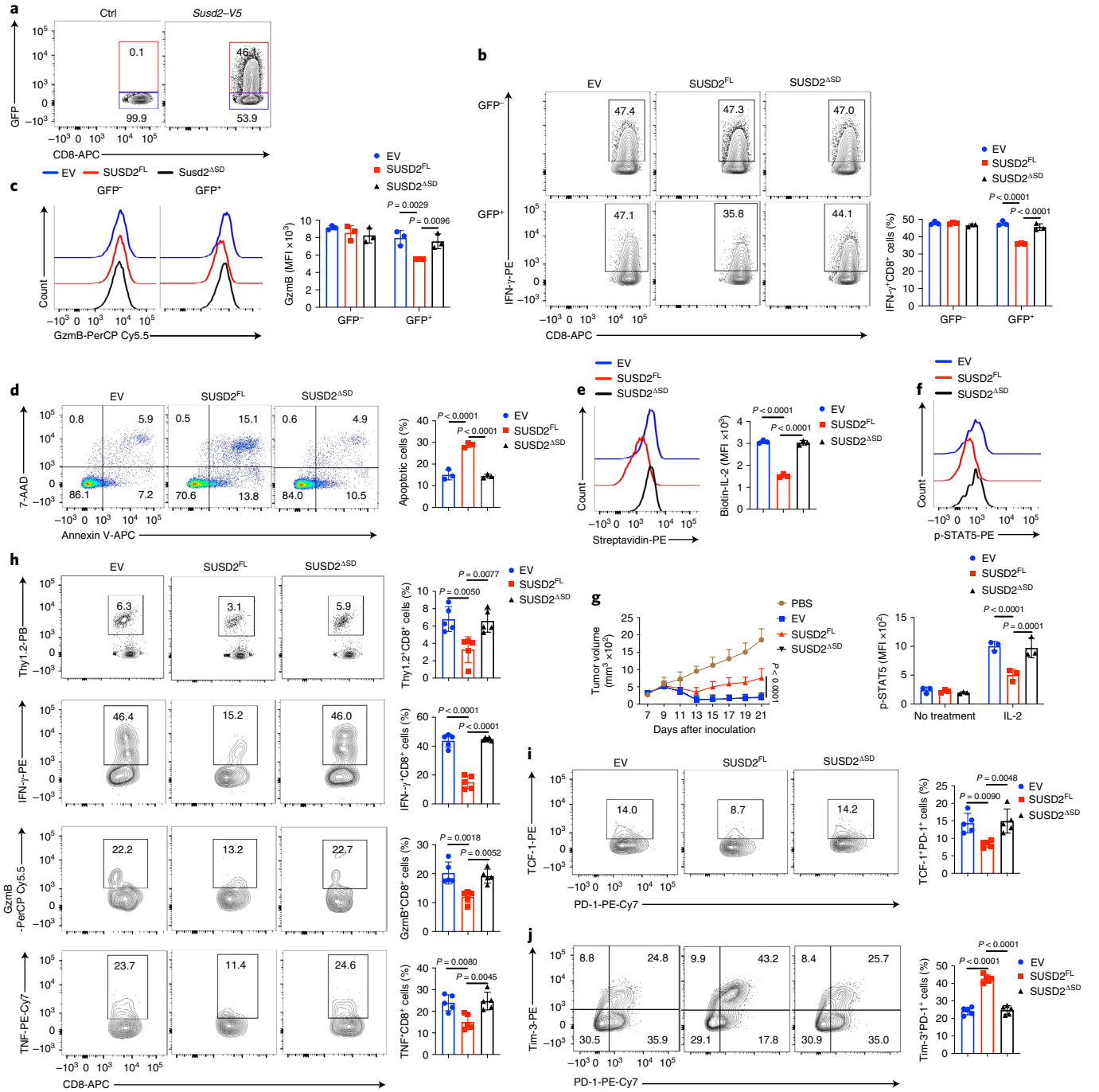

Fig. 6 | SUSD2–IL-2Rα interaction impairs antitumor effector function of CD8⁺ T cells. a, Flow cytometry analysis of GFP in $OVA_{257–264}$-primed *Susd2*$^{-/-}$ OT-I T cells transfected with EV–GFP or SUSD2^{FL}–GFP. **b**-**d**, Flow cytometry of IFN-γ$^+$CD8$^+$ T cells (**b**), GzmB$^+$CD8$^+$ T cells (**c**) and annexin V$^+$7-AAD$^+$CD8$^+$ T cells (**d**) in $OVA_{257–264}$-stimulated *Susd2*$^{-/-}$ OT-I T cells retrovirally transduced with EV–GFP, SUSD2^{FL}–GFP or SUSD2^{ΔSD}–GFP. **e**,**f**, Binding of biotinylated IL-2 assessed by streptavidin staining (**e**) and STAT5 phosphorylation (**f**) in $OVA_{257–264}$-primed *Susd2*$^{-/-}$ OT-I T cells retrovirally transduced with EV–GFP, SUSD2^{FL}-GFP or SUSD2^{ΔSD}-GFP and stimulated with biotin-conjugated IL-2 for 1 h following overnight resting after transduction. **g**, Tumor growth in EG7-bearing Thy1.1 congenic mice at 2, 4, 6, 8, 10, 12 and 14 d after PBS treatment or after -transfer with *Susd2*$^{-/-}$ OT-I T cells transduced with EV–GFP, SUSD2^{FL}–GFP or SUSD2^{ΔSD}–GFP. **h**–**j**, Frequencies of Thy1.2$^+$CD8$^+$ T cells, IFN-γ$^+$CD8$^+$ T cells, GzmB$^+$CD8$^+$ T cells, TNF$^+$CD8$^+$ T cells (**h**), TCF-1$^+$PD-1$^+$CD8$^+$ T cells (**i**) and Tim-3$^+$PD-1$^+$CD8$^+$ T cells (**j**) in EG7 tumors isolated 18 d after EG7 inoculation from Thy1.1 mice that received *Susd2*$^{-/-}$ OT-I T cells transduced with EV–GFP, SUSD2^{FL}–GFP or SUSD2^{ΔSD}–GFP at day 7 after EG7 inoculation. $n = 3$ mice per group (**a**–**f**) and $n = 5$ (**g**–**j**) mice per group. Data are representative of five independent experiments (**a**–**f**) and three independent experiments (**g**–**j**). Statistical significance was determined by two-way ANOVA followed by Tukey's multiple comparisons test (**b**,**c**,**f**,**g**) or one-way ANOVA followed by Tukey's test (**d**,**e**,**h**–**j**) with *P* values noted in the figure. Data represent mean ± s.d.

(SUSD2^{FL}–GFP), SUSD2^{ΔSD}–GFP or empty vector (EV)–GFP with about 50% of transduction efficiency (Fig. 6a), we observed decreased production of IFN-γ and GzmB (Fig. 6b, c) and increased apoptosis (Fig. 6d) in GFP$^+$ OT-I T cells reconstituted with SUSD2^{FL}–GFP, but not with SUSD2^{ΔSD}–GFP compared to cells reconstituted with EV–GFP. Moreover, transduction of *Susd2*$^{-/-}$ OT-I T cells with SUSD2^{FL}–GFP, but not SUSD2^{ΔSD}–GFP, inhibited the binding of biotinylated IL-2 to *Susd2*$^{-/-}$ OT-I T cells (Fig. 6e) and IL-2-induced STAT5 phosphorylation (Fig. 6f). These

https://doi.org/10.1038/s41590-022-01326-8

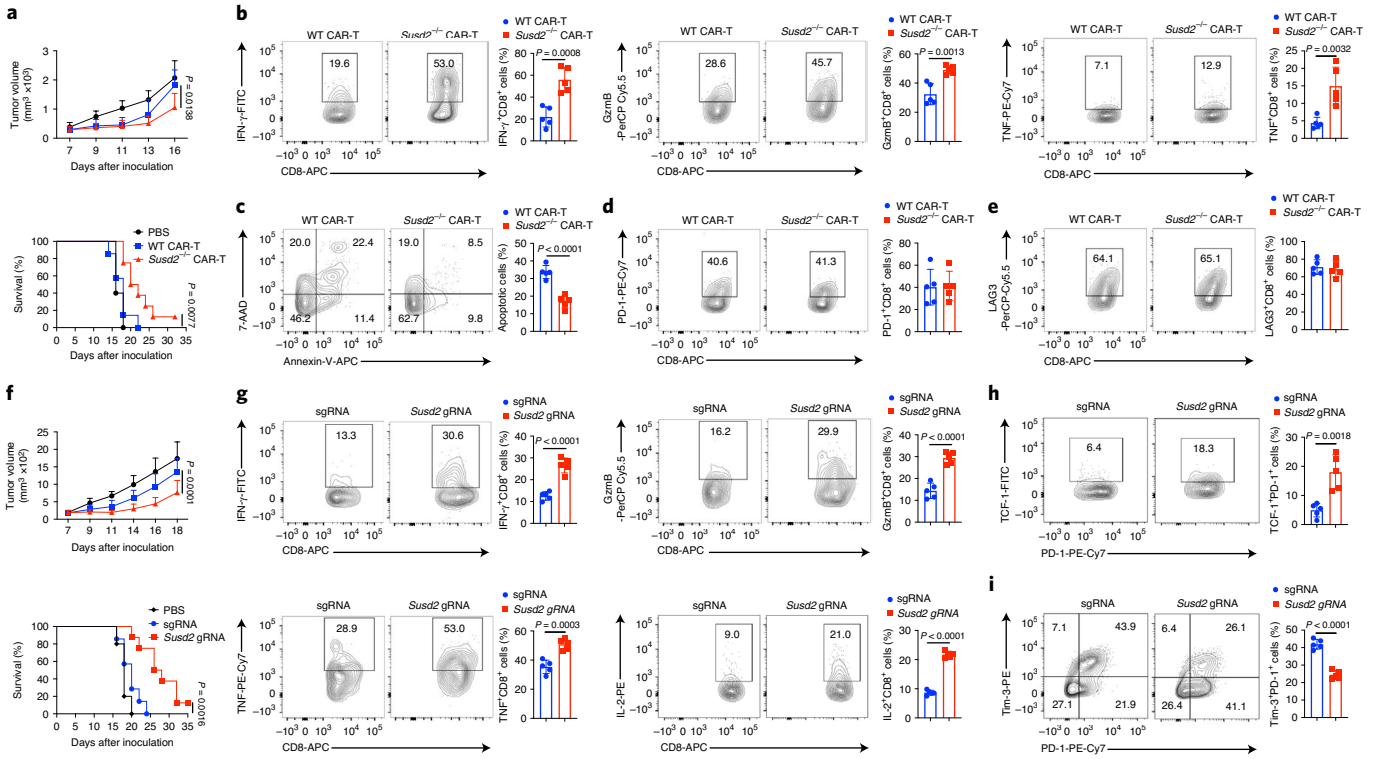

Fig. 7 | Deletion of Susd2 improves antitumor efficacy of CAR T cells. a, Tumor growth and survival in EL4-hCD19 tumor-bearing *Rag2*$^{-/-}$ mice that received adoptive transfer of WT or *Susd2*$^{-/-}$ CAR T cells at day 7 after tumor inoculation. **b**–**e**, Frequencies of IFN-γ^{+}CD8^{+} T cells, GzmB^{+}CD8^{+} T cells, TNF^{+}CD8^{+} T cells (**b**), annexin V^{+}7-AAD^{+}CD8^{+} T cells (**c**), PD-1^{+}CD8^{+} T cells (**d**) and LAG3^{+}CD8^{+} T cells (**e**) in EL4-hCD19 tumors isolated from *Rag2*$^{-/-}$ mice that received WT or *Susd2*$^{-/-}$ CAR T cells at day 18 after tumor inoculation. **f**, Tumor growth and survival in EL4-hCD19-bearing *Rag2*$^{-/-}$ mice that received CAR T cells containing either scrambled gRNA (sgRNA) or *Susd2* gRNA at day 7 after tumor inoculation. **g**–**i**, Frequencies of IFN-γ^{+}CD8^{+} T cells, GzmB^{+}CD8^{+} T cells, TNF^{+}CD8^{+} T cells and IL-2^{+}CD8^{+} T cells (**g**), TCF-1^{+}PD-1^{+}CD8^{+} T cells (**h**) and Tim-3^{+}PD-1^{+}CD8^{+} T cells (**i**) in EL4-hCD19 tumors isolated from *Rag2*$^{-/-}$ mice transferred with sgRNA or *Susd2* gRNA CAR T cells at day 18 after tumor inoculation. $n = 5$–7 (**a**); $n = 5$–8 (**f**); and $n = 5$ mice per group (**b**–**e**, **g**–**i**). Data are representative of three independent experiments (**a**–**e**) and two independent experiments (**f**–**i**). Statistical significance was determined by two-way ANOVA followed by Tukey's multiple comparisons test (**a**,**f**, **top**), log-rank (Mantel–Cox) test survival analysis (**a**,**f**, **bottom**) or two-tailed unpaired Student's *t*-test (**b**–**e**,**g**–**i**) with *P* values noted in the figure. Data represent mean ± s.d.

results suggested that loss of SUSD2 interaction with IL-2Rα ablated its inhibitory effect on CD8^{+} T cell effector function in vitro.

To determine whether the Susd2–IL-2Rα interaction modulated the antitumor effector function of CD8^{+} T cells in vivo, we adoptively transferred Thy1.2^{+}*Susd2*$^{-/-}$ OT-I T cells transduced with SUSD2^{FL}–GFP, SUSD2$^{\Delta SD}$–GFP or EV–GFP into Thy1.1^{+} mice challenged with EG7 tumor cells 7 d before cell transfer. While SUSD2^{FL}–GFP *Susd2*$^{-/-}$ OT-I T cells exhibited impaired capacity to control EG7 tumor growth, SUSD2$^{\Delta SD}$–GFP *Susd2*$^{-/-}$ OT-I T cells controlled tumor growth at levels comparable to EV–GFP *Susd2*$^{-/-}$ OT-I T cells (Fig. 6g). SUSD2^{FL}–GFP, but not SUSD2$^{\Delta SD}$–GFP *Susd2*$^{-/-}$ OT-I T cells had attenuated tumor infiltration, decreased production of IFN-γ, GzmB and TNF (Fig. 6h) and significantly decreased about 42% of CD8^{+} T_{EXP} cell (Fig. 6i) and increased about 77% of CD8^{+} T_{EXT} cells (Fig. 6j) compared to EV–GFP *Susd2*$^{-/-}$ OT-I T cells. This indicated that the SUSD2–IL-2Rα interaction was required for the inhibitory role of SUSD2 on the antitumor effector function of CD8^{+} T cells (Extended Data Fig. 8).

Deletion of Susd2 improves antitumor efficacy of CAR T cells

To evaluate the potential of SUSD2 as an immunotherapy target for cancer, we investigated its role in regulating the antitumor efficacy of human CD19 (hCD19)-targeting chimeric antigen receptor (CAR) T cells. The mouse EL4 thymoma cell line was engineered to express hCD19 (Extended Data Fig. 7a) and wild-type or *Susd2*$^{-/-}$CD8^{+} T cells were retrovirally transduced with a second-generation CAR containing a portion of hCD19 single chain variable fragment (ScFv) fused with the signaling domains from mouse CD28 and a mouse CD3ζ sequence in which the first and third ITAMs (immunoreceptor tyrosine-based activation motifs) had been inactivated[39]. Sorted CAR T cells with a 98% live cell purity were transferred into *Rag2*$^{-/-}$ mice that have been inoculated with EL4-hCD19 tumor cells 7 d before CAR T cell transfer (Extended Data Fig. 7b). While wild-type CAR T cells restrained tumor growth before day 13 after tumor cell inoculation, tumor growth rebounded at day 13, leading to similar survival in *Rag2*$^{-/-}$ mice with or without wild-type CAR T cell transfer (Fig. 7a). Transfer of *Susd2*$^{-/-}$ CAR T cells significantly reduced tumor growth at day 16 after tumor cell inoculation and translated in improved survival compared to wild-type CAR T cells (Fig. 7a). We detected enhanced production of IFN-γ, GzmB and TNF as well as improved cell survival in intratumoral *Susd2*$^{-/-}$ CAR T cells compared to wild-type CAR T cells (Fig. 7b,c). Intratumoral *Susd2*$^{-/-}$ and wild-type CAR T cells had similar expression of PD-1 or LAG3 (Fig. 7d,e). As such, deletion of SUSD2 in CAR T cells lead to an improved antitumor response in an EL4-hCD19 tumor model.

Next, we depleted endogenous *Susd2* in wild-type CAR T cells using Cas9 nucleoprotein (RNP) complex electroporation[40] (Extended Data Fig. 7c). Transfer of *Susd2*-depleted CAR T cells in *Rag2*$^{-/-}$ mice resulted in improved control of EL4-hCD19 tumors and increased survival compared to transfer of wild-type CAR T cells (Fig. 7f). We observed increased production of IFN-γ, GzmB, TNF and IL-2 (Fig. 7g) and increased percentages of TCF1^{+}PD-1^{+}CD8^{+} T_{EXP} cells and decreased percentages of TCF1^{-}PD-1^{+}Tim-3^{+} CD8^{+} T_{EXT} in *Susd2*-depleted CAR T cells compared to wild-type CAR T cells (Fig. 7h,i), suggesting that

therapeutic deletion of SUSD2 improved effector function of CAR T cells and counteracted the differentiation of terminally exhausted CAR T cells.

Discussion

This study showed an inhibitory effect of SUSD2 on IL-2R signaling, consequently leading to an inhibition of the antitumor function of $CD8^+$ T cells. We found that SUSD2 interacted with IL-2Rα via an SD-dependent manner and interfered with IL-2-mediated effector functions of $CD8^+$ T cells. Deletion of SUSD2 in adoptively transferred T_{eff} cells and CAR T cells led to an improved antitumor efficacy, suggesting a targetable relevance of SUSD2 in immunotherapy for cancer.

IL-2 was originally discovered as a T cell growth factor with a robust effect to promote the expansion of cytotoxic $CD8^+$ T cells[6,36]. Clinical studies revealed promising results for IL-2 therapy in patients with cancer[41,42]; however, an intrinsic challenge of IL-2-based cancer immunotherapy is the activation of cytotoxic $CD8^+$ T cells in peripheral sites, which causes undesirable tissue damage. We found that, among various immune cell types, SUSD2 was highly expressed in $CD8^+$ T cells and was further upregulated when $CD8^+$ T cells migrated from the secondary lymphoid organ into the TME. Therefore, based on the inhibitory effect of SUSD2 on IL-2R signaling, blockade of SUSD2 may preferentially enhance the survival and function of antitumor $CD8^+$ T cells and avoid the activation of peripheral $CD8^+$ T cells. Meanwhile, as our current animal model employed a whole-body gene deletion strategy, we are not able to completely rule out potential function of SUSD2 in cellular compartments other than $CD8^+$ T cells. Further development of genetic model with conditional gene deletion is warranted to examine the role of SUSD2 in individual cell types.

Both experimental studies in tumor animal models and clinical cancer studies have characterized $CD8^+$ T cell exhaustion in the TME[43]. With the rapid advancement in scRNA-seq technology, compelling evidence shows the existence of distinct subtypes of exhausted $CD8^+$ T cells, namely TCF-1^+PD-1^+Tim-3^- T_{ExP} cells and TCF-1^-PD-1^+Tim-3^+ T_{ExT} cells[30,31,44]. $CD8^+$ T_{eff} cells with high expression of antitumor effectors, such as IFN-γ and granzymes, are critically required for the execution of the antitumor response[30–32]. Intratumoral $CD8^+$ T_{ExP} cells can either differentiate into CX_3CR1^+ $CD8^+$ T_{eff} cells or T_{ExT} cells via distinct transcriptional, epigenetic and metabolic programs[30,31,44]. One strategy to improve $CD8^+$ T cell antitumor response might be to promote the conversion of T_{ExP} to T_{eff} cells and minimize the differentiation of T_{ExT} cells. IL-2R signaling potently activates the effector responses of $CD8^+$ T cells[7,8] and IL-2 in combination with PD-L1 antibody therapy can rejuvenate T_{ExT} cells in a chronic virus infection model[45]. Therefore, targeting IL-2R signaling, either alone or in combination with other ICB therapies, represents a promising approach to escalate the antitumor function of $CD8^+$ T cells while minimizing T cell exhaustion. Our scRNA-seq assay indicated an increased percentage of $CD8^+$ T_{eff} cells and decreased percentage of T_{ExT} cells in tumor-bearing *Susd2*$^{-/-}$ mice, highlighting a promising therapeutic potential of SUSD2 to reverse T cell exhaustion.

The long-term efficacy of CAR T therapy in cancer is severely limited by the conversion of transferred T_{eff} cells to T_{ExT} cells. An experimental approach to block the terminal exhaustion of CAR T cell would represents a promising strategy to improve the efficacy of CAR T cell therapy. We found that depletion of endogenous *Susd2* gene in wild-type CAR T cells resulted in an improved control of tumor growth, increased effector function and decreased T cell death and terminal exhaustion, providing a promising base for further investigations in human CAR T cells.

SUSD2 is also expressed in certain types of cancers[20–26]. Clinical studies have reported either positive or negative correlations between SUSD2 expression in tumor cells and a positive prognosis in patients with cancer, depending on the type of cancer[20–26]. Further investigations are required to fully characterize the role of SUSD2 in tumor cells. In summary, our results provide a mechanistic link between the SUSD2-modulated IL-2R signaling and the antitumor effector function of $CD8^+$ T cells and expand our current understanding of molecular mechanisms driving immunosuppression in the TME. Considering the rapid advancements in the development of immunotherapy antibodies, blockade of SUSD2 by neutralizing antibody could represents a new therapeutic approach for cancer. Moreover, because SUSD2 modulates $CD8^+$ T cell effector function independently of PD-1, blockade of SUSD2 seems suitable for combinatorial therapy, especially for tumors that are resistant to PD-1 therapy.

Online content

Any methods, additional references, Nature Research reporting summaries, source data, extended data, supplementary information, acknowledgements, peer review information; details of author contributions and competing interests; and statements of data and code availability are available at https://doi.org/10.1038/s41590-022-01326-8.

References

1. Schoenfeld, A. J. & Hellmann, M. D. Acquired resistance to immune checkpoint inhibitors. *Cancer Cell* **37**, 443–455 (2020).
2. Altorki, N. K. et al. The lung microenvironment: an important regulator of tumour growth and metastasis. *Nat. Rev.* **19**, 9–31 (2019).
3. Binnewies, M. et al. Understanding the tumor immune microenvironment (TIME) for effective therapy. *Nat. Med.* **24**, 541–550 (2018).
4. Andrews, L. P., Yano, H. & Vignali, D. A. A. Inhibitory receptors and ligands beyond PD-1, PD-L1 and CTLA-4: breakthroughs or backups. *Nat. Immunol.* **20**, 1425–1434 (2019).
5. Kalbasi, A. & Ribas, A. Tumour-intrinsic resistance to immune checkpoint blockade. *Nat. Rev. Immunol.* **20**, 25–39 (2020).
6. Morgan, D. A., Ruscetti, F. W. & Gallo, R. Selective in vitro growth of T lymphocytes from normal human bone marrows. *Science* **193**, 1007–1008 (1976).
7. Pipkin, M. E. et al. Interleukin-2 and inflammation induce distinct transcriptional programs that promote the differentiation of effector cytolytic T cells. *Immunity* **32**, 79–90 (2010).
8. Kalia, V. et al. Prolonged interleukin-2Rα expression on virus-specific $CD8^+$T cells favors terminal-effector differentiation in vivo. *Immunity* **32**, 91–103 (2010).
9. Boyman, O. & Sprent, J. The role of interleukin-2 during homeostasis and activation of the immune system. *Nat. Rev. Immunol.* **12**, 180–190 (2012).
10. Leonard, W. J., Lin, J. X. & O'Shea, J. J. The γc family of cytokines: basic biology to therapeutic ramifications. *Immunity* **50**, 832–850 (2019).
11. Wang, X., Rickert, M. & Garcia, K. C. Structure of the quaternary complex of interleukin-2 with its α, β, and γc receptors. *Science* **310**, 1159–1163 (2005).
12. Rickert, M., Wang, X., Boulanger, M. J., Goriatcheva, N. & Garcia, K. C. The structure of interleukin-2 complexed with its α receptor. *Science* **308**, 1477–1480 (2005).
13. Boyman, O., Kovar, M., Rubinstein, M. P., Surh, C. D. & Sprent, J. Selective stimulation of T cell subsets with antibody-cytokine immune complexes. *Science* **311**, 1924–1927 (2006).
14. Williams, M. A., Tyznik, A. J. & Bevan, M. J. Interleukin-2 signals during priming are required for secondary expansion of $CD8^+$ memory T cells. *Nature* **441**, 890–893 (2006).
15. Bachmann, M. F., Wolint, P., Walton, S., Schwarz, K. & Oxenius, A. Differential role of IL-2R signaling for $CD8^+$ T cell responses in acute and chronic viral infections. *Eur. J. Immunol.* **37**, 1502–1512 (2007).
16. Malek, T. R. The biology of interleukin-2. *Annu. Rev. Immunol.* **26**, 453–479 (2008).

17. Scott, E. N., Gocher, A. M., Workman, C. J. & Vignali, D. A. A. Regulatory T cells: barriers of immune infiltration into the tumor microenvironment. *Front. Immunol.* **12**, 702726 (2021).
18. Sugahara, T. et al. Isolation of a novel mouse gene, mSVS-1/SUSD2, reversing tumorigenic phenotypes of cancer cells in vitro. *Cancer Sci.* **98**, 900–908 (2007).
19. Souri, M., Kaetsu, H. & Ichinose, A. Sushi domains in the B subunit of factor XIII responsible for oligomer assembly. *Biochemistry* **47**, 8656–8664 (2008).
20. Watson, A. P., Evans, R. L. & Egland, K. A. Multiple functions of sushi domain containing 2 (SUSD2) in breast tumorigenesis. *Mol. Cancer Res.* **11**, 74–85 (2013).
21. Pan, W. et al. CSBF/C10orf99, a novel potential cytokine, inhibits colon cancer cell growth through inducing G1 arrest. *Sci. Rep.* **4**, 6812 (2014).
22. Cai, C. et al. Reduced expression of sushi domain containing 2 is associated with progression of non-small cell lung cancer. *Oncol. Lett.* **10**, 3619–3624 (2015).
23. Sheets, J. N. et al. SUSD2 expression in high-grade serous ovarian cancer correlates with increased patient survival and defective mesothelial clearance. *Oncogenesis* **5**, e264 (2016).
24. Hultgren, E. M., Patrick, M. E., Evans, R. L., Stoos, C. T. & Egland, K. A. SUSD2 promotes tumor-associated macrophage recruitment by increasing levels of MCP-1 in breast cancer. *PLoS ONE* **12**, e0177089 (2017).
25. Zhang, S. et al. Downregulation of endometrial mesenchymal marker SUSD2 causes cell senescence and cell death in endometrial carcinoma cells. *PLoS ONE* **12**, e0183681 (2017).
26. Umeda, S. et al. Expression of sushi domain containing two reflects the malignant potential of gastric cancer. *Cancer Med.* **7**, 5194–5204 (2018).
27. Li, X. et al. Myeloid-derived cullin 3 promotes STAT3 phosphorylation by inhibiting OGT expression and protects against intestinal inflammation. *J. Exp. Med.* **214**, 1093–1109 (2017).
28. McLane, L. M., Abdel-Hakeem, M. S. & Wherry, E. J. CD8 T cell exhaustion during chronic viral infection and cancer. *Annu. Rev. Immunol.* **37**, 457–495 (2019).
29. Miller, B. C. et al. Subsets of exhausted CD8(+) T cells differentially mediate tumor control and respond to checkpoint blockade. *Nat. Immunol.* **20**, 326–336 (2019).
30. Chen, Z. et al. TCF-1-centered transcriptional network drives an effector versus exhausted CD8 T cell-fate decision. *Immunity* **51**, 840–855 (2019).
31. Hudson, W. H. et al. Proliferating transitory T cells with an effector-like transcriptional signature emerge from PD-1(+) stem-like CD8(+) T cells during chronic infection. *Immunity* **51**, 1043–1058 (2019).
32. Zander, R. et al. CD4(+) T cell help is required for the formation of a cytolytic CD8(+) T cell subset that protects against chronic infection and cancer. *Immunity* **51**, 1028–1042 (2019).
33. Lin, H. et al. Host expression of PD-L1 determines efficacy of PD-L1 pathway blockade-mediated tumor regression. *J. Clin. Invest.* **128**, 805–815 (2018).
34. Wen, H., Dou, Y., Hogaboam, C. M. & Kunkel, S. L. Epigenetic regulation of dendritic cell-derived interleukin-12 facilitates immunosuppression after a severe innate immune response. *Blood* **111**, 1797–1804 (2008).
35. Mo, F. et al. An engineered IL-2 partial agonist promotes CD8(+) T cell stemness. *Nature* **597**, 544–548 (2021).
36. Spolski, R., Li, P. & Leonard, W. J. Biology and regulation of IL-2: from molecular mechanisms to human therapy. *Nat. Rev. Immunol.* **18**, 648–659 (2018).
37. Krieg, C., Letourneau, S., Pantaleo, G. & Boyman, O. Improved IL-2 immunotherapy by selective stimulation of IL-2 receptors on lymphocytes and endothelial cells. *Proc. Natl Acad. Sci. USA* **107**, 11906–11911 (2010).
38. Spangler, J. B. et al. Antibodies to interleukin-2 elicit selective T cell subset potentiation through distinct conformational mechanisms. *Immunity* **42**, 815–825 (2015).
39. Chen, J. et al. NR4A transcription factors limit CAR T cell function in solid tumours. *Nature* **567**, 530–534 (2019).
40. Ye, L. et al. A genome-scale gain-of-function CRISPR screen in CD8 T cells identifies proline metabolism as a means to enhance CAR-T therapy. *Cell Metab.* **34**, 595–614 (2022).
41. Lotze, M. T. et al. High-dose recombinant interleukin 2 in the treatment of patients with disseminated cancer. Responses, treatment-related morbidity, and histologic findings. *JAMA* **256**, 3117–3124 (1986).
42. Dudley, M. E. et al. Cancer regression and autoimmunity in patients after clonal repopulation with antitumor lymphocytes. *Science* **298**, 850–854 (2002).
43. Hashimoto, M. et al. CD8 T cell exhaustion in chronic infection and cancer: opportunities for interventions. *Annu Rev. Med.* **69**, 301–318 (2018).
44. Beltra, J. C. et al. Developmental relationships of four exhausted CD8(+) T cell subsets reveals underlying transcriptional and epigenetic landscape control mechanisms. *Immunity* **52**, 825–841 e828 (2020).
45. West, E. E. et al. PD-L1 blockade synergizes with IL-2 therapy in reinvigorating exhausted T cells. *J. Clin. Invest.* **123**, 2604–2615 (2013).

Methods

Cell lines

The 293T (CRL-3216), MC38 (RRID: CVCL_B288), B16-F10 (CRL-6475), EL4 (TIB39), EG7 (CRL-2113), Jurkat (TIB152) and Phoenix Eco Packaging cell (CRL-3214) were purchased from the American Type Culture Collection (ATCC), B16-OVA (SCC420) was obtained from Sigma-Aldrich and Platinum-E (Plat-E) (RV-101) was obtained from Cell Biolabs. The 293T, MC38 and B16-OVA cells were cultured in DMEM (Gibco) supplemented with 10% fetal bovine serum (FBS; Sigma-Aldrich), 1% glutamine (Gibco), 1% sodium pyruvate, 1% non-essential amino acids (Gibco), 100 IU ml^{-1} penicillin and 100 μg ml^{-1} streptomycin (Gibco). EL4, EG7, B16-F10 and Jurkat cells were grown in RPMI-1640 (Gibco) supplemented with 10% FBS, 1% glutamine, 1% sodium pyruvate, 1% non-essential amino acids, 100 IU ml^{-1} penicillin and 100 μg ml^{-1} streptomycin. All cell lines were maintained at 37 °C and 5% CO_2. Buffy coats from healthy donors were purchased from the Gulf Coast Regional Blood Center and PBMCs were isolated by Ficoll-Paque (17-1440-03, GE Healthcare) density centrifugation.

Mice

Susd2$^{-/-}$ mice were generated by Cyagen Biosciences using a CRISPR/Cas9-mediated genome engineering strategy (details in Extended Data Fig. 1a). C57BL/6J (000664), Thy1.1 (000406), *Rag2*$^{-/-}$ (008449) and OT-I (003831) mice were obtained from the Jackson Laboratory. OT-II mice have been previously described[46]. *Susd2*$^{-/-}$ OT-I and *Susd2*$^{-/-}$ OT-II mice were generated by crossing *Susd2*$^{-/-}$ with OT-I and OT-II mice, respectively. All mice were housed in standard rodent micro-isolator cages and acclimated to study conditions for at least 7 d before manipulation. Mice were kept in animal rooms maintained on 12-h light–dark cycle, temperature and humidity-controlled, between 68–74 °F and 30–70%, respectively. All in vivo experiments were performed in according with the guidelines established by The Ohio State University and National Institute of Health Guide for the Care and Use of Laboratory Animals and the Institutional Animal Care and Use Committee (protocol no. 2018A00000022-R1).

Tumor cell inoculation

Eight to ten-week-old male and female mice were inoculated subcutaneously with 1×10^6 MC38, EG7 or B16-OVA cells in the right flank. For adoptive T cell transfer experiments, 1×10^6 EG7 cells were inoculated subcutaneously into Thy1.1 mice (day 0). On day 7 after inoculation, mice were adoptively transferred with 4×10^6 WT or *Susd2*$^{-/-}$ OT-I T cells via tail vein. For CAR T transfer experiments, 1×10^6 EL4-hCD19 cells were inoculated subcutaneously into *Rag2*$^{-/-}$ mice (day 0). On day 7 after inoculation, mice were injected with 5×10^6 WT or *Susd2*$^{-/-}$ CAR T cells. For $CD8^+$ T cell depletion, WT or *Susd2*$^{-/-}$ mice were treated with 200 μg of control IgG (clone LTF-2, Bio X cell) or CD8 antibody (clone 2.43, Bio X cell) at 0, 7 and 14 d after tumor inoculation. For PD-L1 or PD-1 blockade, WT or *Susd2*$^{-/-}$ mice were intraperitoneally injected with 250 μg of control IgG or PD-L1 antibody (clone 10 F.9G2, Bio X Cell) or PD-1 antibody (clone RMP1-14, Bio X Cell) at 7, 10 and 13 d after tumor inoculation. For IL-2 antibody complex treatment, mIL-2 (1.5 μg, Peprotech) complexed with either IL-2 antibody (7.5 μg; JES6-1A12, Bio X cell) or IL-2/IL-2 antibody (7.5 μg; S4B6-1, Bio X cell) was administered intraperitoneally at 7, 9, 11 and 13 d after tumor inoculation. Tumor volumes were calculated using the formula mm^3 = (length × width × width / 2).

Flow cytometry

Tumors were minced into small fragments and digested with 1 mg ml^{-1} collagenase IV and 50 U ml^{-1} DNase I for 30 min at 37 °C. Samples were mechanically disaggregated and filtered with 70-μm cell strainers. Single-cell suspensions were treated with purified CD16/32 antibody (clone 93; BioLegend), and then stained with fluorochrome-conjugated antibodies, including CD11b, F4/80, CD11c, Ly6C, Ly6G, CD3, CD4, CD8, CD8, CD25, Thy1.1, Thy1.2, NK1.1, CD19, PD-1 and LAG3. For intracellular staining of p-STAT5, cells were fixed with 2% paraformaldehyde for 10 min at room temperature and then incubated in pre-chilled methanol for 20 min at 4 °C for permeabilization. Cells were washed three times with PBS containing 2% FBS and 1 mM EDTA and then stained with p-STAT5 antibody. For intracellular cytokine staining of tumor-infiltrating lymphocytes, cells were stimulated in vitro with PMA (50 ng ml^{-1}, Sigma-Aldrich) and ionomycin (500 ng ml^{-1}, Sigma-Aldrich) in the presence of GolgiPlug and GolgiStop (BD Biosciences) for 4 h, and then surface stained as aforementioned. Cells were then fixed and permeabilized using BD Cytofix/Cytoperm (BD Biosciences) and stained with IFN-γ, GzmB, TNF and IL-2 antibodies. For intranuclear Foxp3 or TCF-1 staining, single-cell suspensions were stained with antibodies against cell-surface antigens as aforementioned, fixed and permeabilized using Foxp3 Fix/Perm Buffer kit (BioLegend), followed by staining with Foxp3 antibody or TCF-1 antibody. For cell apoptosis analysis, cells were resuspended in the annexin V Binding Buffer and then stained with annexin V and 7-AAD viability solution (BioLegend) for 15 min at 25 °C.

To characterize $CD8^+$ cells in the TME, multi-dimensional flow cytometry assay with a panel of 32 lineage- and T cell state-specific markers (CD45, CD3, CD8, CD4, CD11b, NK1.1, Foxp3, Tim-3, PD-1, CD25, CD62L, CD69, CD44, Lag3, Vista, TIGIT, CD27, CD38, CD39, KLRG1, ICOS. CD95, CD103, CXCR3, TOX, TCF-1, Ki67, EOMES, IFN-γ, TNF and GzmB) was performed, as previously described[47]. Data were acquired in a 5-Laser Cytek Aurora System. Analysis was performed using OMIQ data analysis software (www.omiq.ai) (Omiq). UMAP was applied for dimension reduction and visualization of the data after concatenating all samples. Cells were then clustered based on their marker expression using the FlowSOM package[48]. Heat maps of median marker expression were generated to further understand the features of each cluster. Differences in the abundance of the clusters between the two groups were determined with EdgeR.

Cell sorting

$CD4^+$, $CD8^+$, $CD11b^+$ and $CD19^+$ cells were sorted from mouse splenocytes. Human $CD4^+$, $CD8^+$, $CD14^+$ and $CD19^+$ cells were sorted from PBMCs. Mouse T_{reg} cells were isolated using the Mouse $CD4^+CD25^+$ Regulatory T Cell Isolation kit (130-091-041; Miltenyi). Human T_{reg} cells were isolated from PBMCs by EasySep Human $CD4^+CD127^{low}CD25^+$ Regulatory T Cell Isolation kit (18063; STEMCELL Technologies). Cells were sorted using a 100-μm chip on a MA900 Multi-Application Cell Sorter (SONY) in PBS with 2% FBS.

scRNA-seq

MC38 tumor single-cell suspensions were stained with 7-AAD and CD45 antibody and sorted (BD FACSAria Fusion Cell Sorter). Live $CD45^+$ cells were processed using the inDrops V3 scRNA-seq platform, as previously described[49]. inDrops Libraries were sequenced on the NextSeq Illumina Platform, paired-end mode. The raw sequences (FASTQ format; four WT and four KO) were aligned and quantified using the CellRanger (v.3.0.2) pipeline against the pre-built 10x mouse reference genome (mm10). For each dataset, a cell was considered as low quality or abnormal and removed based on (1) fewer than 200 expressed genes; (2) fewer than 200 or higher than 4,000 total features; and (3) mitochondria content higher than 90%. We then performed the integrative analysis using the Seurat (v.3.0) pipeline. Data integration was performed on the top 2,000 highly variable genes in each sample via canonical correlation analysis. Cell clusters were identified using the top five principal components (PCs) with a resolution of 0.5 in Louvain clustering. All cell clusters were manually annotated according to the expression of curated marker genes. Differentially expressed genes (DEGs) were identified in each cell cluster using the Wilcoxon rank test built in Seurat, with log-fold change as 0.25 and adjusted *P* value as 0.05. We further subset those cells with *Cd8a*, *Trbc1* and *Trbc2* expression from the integrated data. The subset data was re-scaled and re-clustered

with the top five PCs and a resolution of 0.2 in Louvain clustering, and further annotated as T_N cells, T_{eff} cells, T_{ExP} cells and T_{ExT} cells based on manually curated $CD8^+$ T cell markers. DEGs in the subset data were identified similarly as described above.

Bulk RNA-seq

$CD8^+$ T cells were isolated by the EasySep Mouse $CD8^+$ T Cell Isolation kit (STEMCELL Technologies) from total splenocytes of either WT or *Susd2*$^{-/-}$ OT-I mice left untreated or stimulated with $OVA_{257–264}$ for 3 d. RNA was extracted using TRIzol Reagent (Invitrogen) and were further quantified using Qubit Fluorometer and those with RNA integrity number values >7 were used for RNA isolation using NEBNext Poly mRNA Magnetic Isolation Module (E7490L, New England Biolabs). Subsequently, purified mRNAs were fragmented for 10 min. cDNAs were synthesized and amplified for 12 PCR cycles using NEBNext Ultra II Directional (stranded) RNA Library Prep kit for Illumina (E7760L; NEB) with NEBNext Multiplex Oligos Index kit (6442L; NEB). Distributions of the template length and adaptor-dimer contamination were assessed using an Agilent 2100 Bioanalyzer and High Sensitivity DNA kit (Agilent Technologies). The concentration of cDNA libraries was determined using Invitrogen Qubit dsDNA HS reagents and read on a Qubit Fluorometer (Thermo Fisher Scientific), and cDNA libraries were paired-end 150-bp format sequenced on a NovaSeq 6,000 SP system (Illumina). Bulk RNA-seq profiling was performed on eight samples (four WT and four knockout (KO)). Quality control and data trimming of the raw sequences were performed via fastp (v.0.23.2), and reads alignment was performed using HISAT2 (v.2.1.0) to map sequence to the mouse reference (*Mus musculus*. GRCm38.99). SamTools (v.1.10) was used to convert and sort bam files, and subread (v.2.0.1) was used to quantify reads to generate gene expression count matrix. DEG analysis was performed using DESeq2 (v.1.32.0). Genes with log-fold change >1.5 and *P* values <0.05 were considered as DEGs in each comparison.

Plasmids and molecular cloning

Commercially available expression plasmids include *SUSD2* (OHu27875) from GenScript, *Susd2* (MmCD00315635) from the Dana-Farber/Harvard Cancer Center DNA Resource Core[50], *IL2RA*–*eGFP* (86055) from Addgene, pCMV3-SP-N-Flag–*mIl2ra* (MG50292-NF) and pCMV3-C-Myc-*MUC4* (HG16066-CM) from Sino Biological. To generate the retrovirus vector expressing *SUSD2*, *Susd2* or *Susd2* with the deletion of SD (SUSD2$^{\triangle SD}$), *SUSD2* and *Susd2* complementary DNA were subcloned into the pLVX–mCherry–N1 (Clontech 632562) or pMSCV-IRES–GFP II (pMIG II, Addgene 52107) with V5 and His tag. To generate Flag–*IL2RA*, *IL2RA* cDNA were subcloned into p3×Flag–CMV-7.1 vector. All primers used for cloning are listed in Supplementary Table 6. To generate IL2RA$^{\triangle SD1}$ or IL2RA$^{\triangle SD2}$ mutant, Phusion Site-Directed mutagenesis kit was used according to the manufacturer's instructions (Thermo Fisher Scientific). Primers for mutagenesis PCR are listed in Supplementary Table 7. All cloned genes were checked by sequencing.

Retroviral transduction of T cells

For retrovirus generation, Plat-E cells were seeded into 10-cm dishes overnight. On the following day, plasmid encoding pMIG II EV, pMIG II-SUSD2^{FL} or pMIG II-SUSD2$^{\triangle SD}$ and packaging plasmid pCL-Eco (Addgene 12371) were mixed along with polyethylenimine (PEI) at a 3:1 PEI:DNA ratio and added into the Plat-E cells overnight. Medium was then changed and viral supernatant was collected twice in the following 72 h. Retroviral supernatants were concentrated by PEG 8000 and immediately stored at −80 °C. For retroviral transduction, OT-I T cells or Jurkat cells were plated in six-well plates, OT-I cells stimulated with 1 μg ml^{-1} $OVA_{257–264}$ for 24 h. Viral supernatant (1:1 vol/vol ratio) and 8 μg ml^{-1} polybrene (Sigma-Aldrich) were added. Spinfection was performed at 32 °C for 2 h at 800*g*. Medium was changed after 2 h. Transduced OT-I T cells were cultured for another 48 h with $OVA_{257–264}$ and tested in functional assays.

Antigen-presenting assay

BMDCs were loaded with 1 μg ml^{-1} $OVA_{257–254}$ at 37 °C for 2 h, then washed three times with PBS to remove excessive peptide. OT-I T cells were collected from spleens of WT or *Susd2*$^{-/-}$ mice by $CD8^+$ T Cell Enrichment kit (Miltenyi) and then co-cultured with peptide-pulsed WT or *Susd2*$^{-/-}$ BMDCs at a 5:1 ratio in 96-well plates. In some experiments, IL-2 (JES6-1A12), IL-2Rα (PC61) or IL-2Rβ (TM-β1) blocking antibody was added to the cocultures at a concentration of 10 μg ml^{-1}.

FACS-based in vitro killing assay

MC38, EG7 and B16-OVA cells were labeled with CFSE (C34554; Thermo Fisher Scientific), MC38 cells were pulsed with $OVA_{257–264}$ peptides at 1 μg ml^{-1} for 1 h and used as target cells. In vitro activated WT or *Susd2*$^{-/-}$ OT-I cells were collected and incubated with peptide-pulsed MC38, EG7 and B16-OVA cells at different ratios for 4 h. The percentage of dead cells were measured with 7-AAD staining.

In vitro T_{reg} cell suppression assay

A total of 1 × 10^5 CFSE-labeled naive T ($CD4^+CD25^-$) cells were stimulated with 1 μg ml^{-1} anti-CD3 antibody and 1 μg ml^{-1} anti-CD28 antibody. T_{reg} cells from WT and *Susd2*$^{-/-}$ mice were isolated with the Mouse $CD4^+CD25^+$ Regulatory T Cell Isolation kit (130-091-041, Miltenyi), and added to the culture to achieve T_{reg}/$CD4^+$ T cell ratios of 0.0625:1 to 1:1. $CD4^+$ T cells only, without T_{reg} cells, were used as a positive control for T cell proliferation. Three days after stimulation, CFSE dilution of $CD4^+$ T cells were analyzed by FACS assay.

IL-2-binding assay

The 1 × 10^6 WT or *Susd2*$^{-/-}$ OT-I T cells were incubated with indicated concentration of biotinylated IL-2 (ACRO Biosystems) in 100 μl PBS, 0.1% BSA for 20 min at 4 °C. Cells were washed three times with PBS and stained with streptavidin-PE (BioLegend) for 30 min at 4 °C. Parallel aliquots of cells were pre-incubated with unlabeled IL-2 (500 ng ml^{-1}, Peprotech). FACS analysis was carried out on BD FACSCanto II Flow Cytometry (BD Biosciences).

RT–PCR

Total RNA was extracted by using TRIzol reagent (Invitrogen). cDNA was synthesized with Moloney murine leukemia virus reverse transcriptase (Invitrogen) at 38 °C for 60 min. RT–PCR was performed using iTaq Universal SYBR Green Supermix (Bio-Rad) in CFX Connect Real-Time PCR Detection System (Bio-Rad). The fold difference in mRNA expression between treatment groups was determined by $^{\triangle\triangle}$Ct method. The primer pair sequences of individual genes are listed in Supplementary Table 8.

Immunoprecipitation and immunoblotting

For IP, cells were lysed in RIPA buffer supplemented with Protease Inhibitor Cocktail. Total protein extracts were incubated with goat anti-V5 agarose (S190-119; Bethyl Laboratories) or anti-Flag M2 Affinity Gel (A2220; Sigma-Aldrich) overnight at 4 °C under gentle agitation. Samples were washed five times with cold RIPA buffer. To elute proteins from the beads, samples were incubated with 30 μl of SDS sample buffer at 95 °C for 10 min. Protein content in the supernatant was analyzed by immunoblotting. For immunoblotting, electrophoresis of proteins was performed by using the NuPAGE system (Invitrogen) according to the manufacturer's protocol. Primary antibodies for immunoblotting included SUSD2 antibody (HPA004117) and FLAG M2-HRP (A8592, Sigma-Aldrich), phospho-Stat5 antibody (Tyr694) (9351, CST), Stat5 (9363, CST), IL-2Rα antibody (AF2438-SP, R&D), IL-2Rα (sc-365511), IL-2Rβ (sc-393093) and IL-15Rα (G-3) antibodies from Santa Cruz Biotechnology, V5-HRP (A00877, GenScript) and γ chain antibody (ab273023, Abcam).

Mass spectrometry assay of SUSD2 interactome

High-resolution/accurate mass-based quantitative proteomics strategy was employed to identify protein–protein interactions. Briefly,

immunoprecipitated (anti-V5) Susd2 complex from retrovirus-infected *Susd2*$^{-/-}$ OT-I T cells was boiled with SDS buffer followed by Suspension Trapping based on-filter digestion, as described previously[51]. The digests were desalted using C18 StageTips, dried in a SpeedVac and then resuspended in 20 µl LC buffer A (0.1% formic acid in water) for LC–MS/MS analysis. The analysis was performed using an Orbitrap Eclipse MS (Thermo Fisher Scientific) coupled with an Ultimate 3000 nanoLC system and a nanospray Flex ion source (Thermo Fisher Scientific). Peptides were first loaded onto a trap column (PepMap C18; 2 cm × 100 µm I.D.) and then separated by an analytical column (PepMap C18, 3.0 µm; 20 cm × 75 mm I.D.) using a binary buffer system (buffer A, 0.1% formic acid in water; buffer B, 0.1% formic acid in acetonitrile) with a 165-min gradient (1% to 25% buffer B over 115 min; 25% to 80% buffer B over 10 min; back to 2% B in 5 min for equilibration after staying on 80% B for 15 min). MS data were acquired in a data-dependent top-12 method with a maximum injection time of 20 ms, a scan range of 350 to 1,800 Da, and an automatic gain control target of 1×10^6. MS/MS was performed via higher energy collisional dissociation fragmentation with a target value of 5×10^5 and maximum injection time of 100 ms. Full MS and MS/MS scans were acquired by Orbitrap at resolutions of 60,000 and 17,500, respectively. Dynamic exclusion was set to 20 s. Protein identification and quantitation were performed using the MaxQuant-Andromeda software suite (v.1.6.3.4) with most of the default parameters[52]. A UniProt mouse database (17,089 sequences) was used for the protein identification. Other parameters include: trypsin as an enzyme with maximally two missed cleavage sites; protein N-terminal acetylation and methionine oxidation as variable modifications; cysteine carbamidomethylation as a fixed modification; peptide length must be at least seven amino acids. False discovery rate was set at 1% for both proteins and peptides.

CAR T cell transfer

The EL4-hCD19 cell line was constructed by transfecting the EL4 cells with an MMLV retrovector carrying hCD19 with the deletion of its intracellular domain. The plasmid was packaged in the Phoenix Eco cell line and viral supernatant was collected 48 h after transfection. After viral transduction, EL4-hCD19 were sorted to achieve the positive clone >95%. To generate hCD19-targeting CAR T cells, the CAR construct was pieced together using portions of hCD19 ScFv, and portions of the murine CD28 and CD3ζ sequences (with first and third ITAMs (immunoreceptor tyrosine-based activation motifs) of the CD3-ζ molecule inactivated), and cloned into an MSGV retrovector, as previously described[53]. The retroviral vector was transfected to the Phoenix Eco cell line. The collection, stimulation and transfection of T cells were conducted. In brief, T cells were isolated from spleens of WT or *Susd2*$^{-/-}$ mice using the EasySep Mouse T Cell Isolation kit (STEMCELL Technologies), and then stimulated by concanavalin A in IMDM (Gibco) with 50 µM 2-mercaptoethanol, 50 U ml^{-1} IL-2, 10 ng ml^{-1} IL-7 and 10 ng ml^{-1} IL-15 at 37 °C for 24 h. On the following day, viral supernatant was spun at 2,000*g*, 32 °C, for 2 h on RetroNectin (Takara Bio)-coated plate. Activated T cells were loaded to the plate and expanded for 2–3 d.

Deletion of endogenous *Susd2* gene in WT CAR T cells was achieved by Cas9 nucleoprotein (RNP) complex electroporation using the Neon Transfection System (MPK5000; Thermo Fisher Scientific), as previously described[40]. Before electroporation, *Susd2* crRNA (AGTGCCGTAGTATTGCCAAT) or negative control crRNA (1072544; IDT) was mixes with Alt-R tracrRNA (1075927; IDT) at 1:1 ratio (final concentration was 44 µM), heat at 95 °C for 5 min, cooled to 78 °C with −2 °C/second ramp rate, 78 °C for 10 min, cooled down to 25 °C with −0.1 °C s^{-1} ramp rate, 25 °C for 5 min. Cas9 protein (3 µg, A36498; Thermo Fisher Scientific) was mixed with 1.3 µl annealed crRNA:tracrRNA duplex and incubated at room temperature for 20 min. Then, 5×10^5 of expanded CAR T cells were resuspended in 9 µl Buffer R per electroporation, and then mixed with RNP complex and 2 µl Alt-R Cas9 Electroporation Enhancer (2075915; IDT). Then, 10 µl of cell:RNP mixture was loaded into the Neon pipette without any bubbles. The tip of the loaded Neon pipette was inserted into the pipette station. The setup of the electroporation parameter was 1,400 V, 50 ms for 1 plus. After electroporation, cells were transferred to a 24-well plate with prewarmed medium and cultured overnight. At 24 h after electroporation, *Susd2*$^{-/-}$ CAR T cells were sorted by using a 100-µm chip on a MA900 Multi-Application Cell Sorter (SONY).

Statistics analysis

Data were analyzed on GraphPad Prism 8 (GraphPad Software) and R software v.4.1.2. The statistical tests, *n* values, replicate experiments and *P* values are all indicated in the figures and/or legends. *P* values were calculated using two-tailed Student's *t*-test, one-way ANOVA or two-way ANOVA with Tukey's multiple comparisons test, log-rank (Mantel–Cox) test for Kaplan–Meier survival analysis, two-way ANOVA with Sidak's multiple comparisons test or Tukey's multiple comparisons test, Hypergeometric test and adjusted with Benjamini–Hochberg method correction and two-sided Wilcoxon's rank-sum test and adjusted with Bonferroni's correction. Differences between groups are shown as the mean ± s.d.

Data distribution was assumed to be normal but this was not formally tested.

Reporting summary

Further information on research design is available in the Nature Research Reporting Summary linked to this article.

Data availability

ScRNA-seq and bulk RNA-seq data reported in this paper are accessible at the Gene Expression Omnibus under accession numbers GSE210704 and GSE212179, respectively. MS data have been deposited in an international public repository (MassIVE proteomics repository at https://massive.ucsd.edu/) under dataset accession number MSV000087205. There are no restrictions for data availability. Source data are provided with this paper.

References

46. Wen, H., Lei, Y., Eun, S. Y. & Ting, J. P. Plexin-A4-semaphorin 3A signaling is required for Toll-like receptor- and sepsis-induced cytokine storm. *J. Exp. Med.* **207**, 2943–2957 (2010).
47. Kwon, H. et al. Androgen conspires with the CD8(+) T cell exhaustion program and contributes to sex bias in cancer. *Sci. Immunol*. https://doi.org/10.1126/sciimmunol.abq2630 (2022).
48. Van Gassen, S. et al. FlowSOM: using self-organizing maps for visualization and interpretation of cytometry data. *Cytom. A* **87**, 636–645 (2015).
49. Zilionis, R. et al. Single-cell barcoding and sequencing using droplet microfluidics. *Nat. Protoc.* **12**, 44–73 (2017).
50. Zuo, D. et al. PlasmID: a centralized repository for plasmid clone information and distribution. *Nucleic Acids Res.* **35**, D680–D684 (2007).
51. Lin, Y. H. et al. Self-assembled STrap for global proteomics and salivary biomarker discovery. *J. Proteome Res.* **18**, 1907–1915 (2019).
52. Tyanova, S., Temu, T. & Cox, J. The MaxQuant computational platform for mass spectrometry-based shotgun proteomics. *Nat. Protoc.* **11**, 2301–2319 (2016).
53. Kochenderfer, J. N., Yu, Z., Frasheri, D., Restifo, N. P. & Rosenberg, S. A. Adoptive transfer of syngeneic T cells transduced with a chimeric antigen receptor that recognizes murine CD19 can eradicate lymphoma and normal B cells. *Blood* **116**, 3875–3886 (2010).

Acknowledgements

We thank members of the Wen laboratory for discussion; Y. Wan for critical feedback; M. Croft for the OT-II mice; Y. Fu for the MC38 cell line; Y. Yu from the University of Delaware Mass Spectrometry Core Facility for the assistance of mass spectrometry assay; P. Yan and

X. Chen from the Genomics Shared Resource at the Ohio State University for the assistance of bulk RNA-seq and scRNA-seq assay. This work was supported by National Institutes of Health grants R01GM135234 and R01AI162779 (H.W.), R01AI077283 and R01CA262089 (Z.L.), R01GM131399 (Q.M.), R01DE026728 (Y.L.), R01AI134972 (K.J.O.) and The Ohio State University Comprehensive Cancer Center Intramural Research Program (A.M., D.M.J., K.H. and H.W.).

Author contributions

H.W. designed the experiments, supervised the study and interpreted the data. B.Z., W.G., J.C., M.V., H.D., Z.L., T.O. and D.M.J. performed experiments and provided intellectual input. A.M. and Q.M. performed key scRNA-seq analysis and provided intellectual input. L.W. and M.L. performed CAR T cell experiment and provided intellectual input. Y.L.L., K.J.O., G.X., D.P.C., K.H. and Z.L. contributed intellectual input and generated critical reagents. H.W. wrote the manuscript.

Competing interests

The authors declare no competing interests.

Additional information

Extended data is available for this paper at https://doi.org/10.1038/s41590-022-01326-8.

Supplementary information The online version contains supplementary material available at https://doi.org/10.1038/s41590-022-01326-8.

Correspondence and requests for materials should be addressed to Haitao Wen.

Peer review information *Nature Immunology* thanks Ping-Chih Ho and the other, anonymous, reviewer(s) for their contribution to the peer review of this work. Primary Handling Editor: Ioana Visan, in collaboration with the *Nature Immunology* team. Peer reviewer reports are available.

https://doi.org/10.1038/s41590-022-01326-8

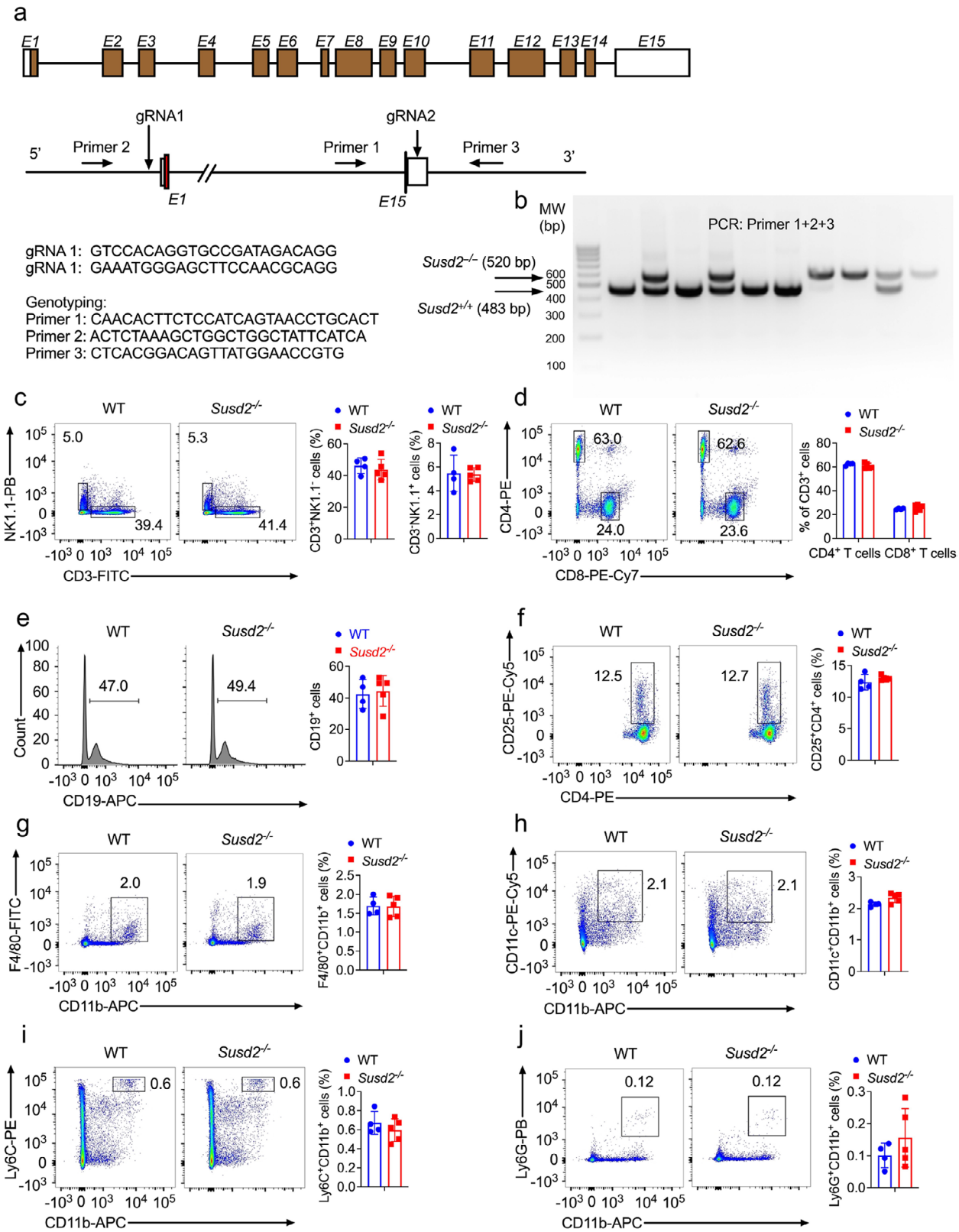

Extended Data Fig. 1 | *Susd2*$^{-/-}$ mice show no change in global immune cell populations at steady state. a, Cartoon of the strategy to generate *Susd2*$^{-/-}$ mice with a CRISPR/Cas9-mediated genome engineering strategy. The sequences of two guide RNA and the primers used for genotyping were shown. **b**, Genotyping results for WT or *Susd2*$^{-/-}$ alleles. **c-j**, Flow cytometry analysis of T cells ($CD3^+$) and natural killer cells ($NK1.1^+$) (**c**), $CD4^+$ and $CD8^+$ T cells (**d**), regulatory T cells in naïve status ($CD4^+CD25^+$) (**f**), macrophage ($CD11b^+F4/80^+$) (**g**), conventional dendritic cells ($CD11b^+CD11c^+$) (**h**), monocytes ($CD11b^+Ly6C^+$) (**i**), neutrophils ($CD11b^+Ly6G^+$) (**j**), and histogram of B cells ($CD19^+$) (**e**) in spleen from wild-type and *Susd2*$^{-/-}$ mice were. **c-j**, WT, $n = 4$ mice, *Susd2*$^{-/-}$, $n = 5$ mice. **b-j**, data are representative of three independent experiments. Statistical significance was determined by two-tailed, unpaired Student's *t*-test, there is no significant difference between WT and *Susd2*$^{-/-}$ in **c-j** ($P > 0.05$). All data are mean ± SD.

https://doi.org/10.1038/s41590-022-01326-8

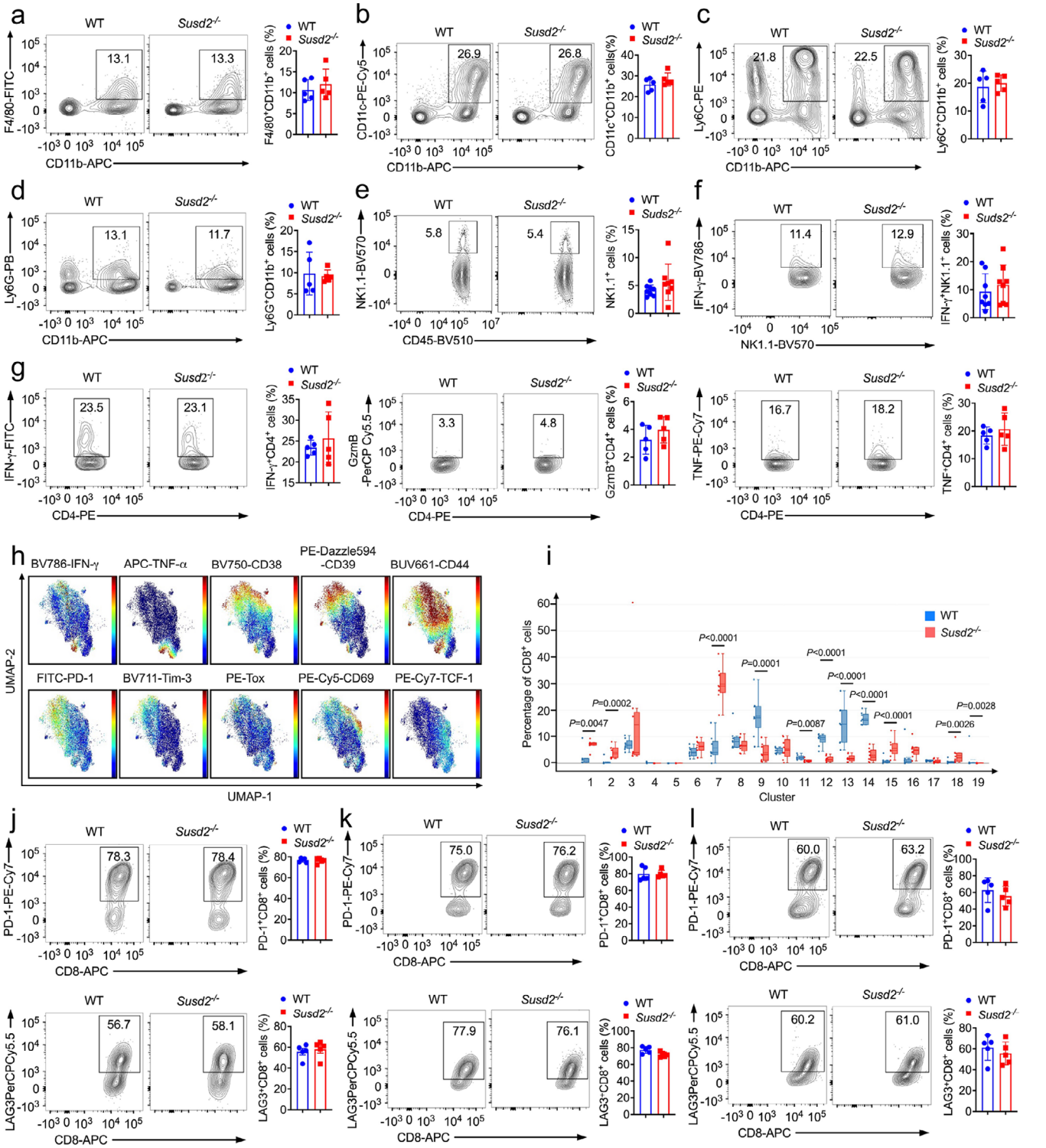

Extended Data Fig. 2 | *Susd2* deficiency does not affect intratumoral myeloid cells, NK cells and CD4$^+$ T cells. a-g, Flow cytometry analysis of CD11b$^+$F4/80$^+$ macrophages (**a**), CD11b$^+$CD11c$^+$ dendritic cells (**b**), CD11b$^+$Ly6C$^+$ monocytes (**c**), CD11b$^+$Ly6G$^+$ neutrophils (**d**), NK1.1$^+$ NK cells (**e**), IFN-γ$^+$NK1.1$^+$ NK cells (**f**), IFN-γ$^+$CD4$^+$, GzmB$^+$CD4$^+$ and TNF$^+$CD4$^+$ T cells (**g**) in MC38 tumor isolated from WT or *Susd2*$^{-/-}$ mice at Day 18. **h,i**, Spectral flow cytometry analysis of intratumor CD8$^+$ T cells from WT and *Susd2*$^{-/-}$ mice at day18 post MC38 tumor inoculation. UMAP of individual marker expression patterns (**h**) and frequencies of individual clusters of WT and *Susd2*$^{-/-}$ samples (**i**), Boxes represent median and 25th to 75th percentiles, whiskers are minimum to maximum values excluding outliers (two-sided Wilcoxon's rank-sum *P* value). **j-l**, Flow cytometry analysis of PD-1$^+$CD8$^+$ T cells and LAG-3$^+$CD8$^+$ T cells in MC38 (**j**), EG7 (**k**) or B16-OVA (**l**) tumors isolated from WT or *Susd2*$^{-/-}$ mice at day 18 post tumor inoculation. **a**–**d**,**g**,**j**-**l**, $n = 5$, **e**,**f**,**i**, $n = 8$. *n*, number of mice per group. a–d,**g**,**j**,**k**,**l**, data are representative of three independent experiments, **e**,**f**,**i**, data are representative of two independent experiments. **a**-**g**, **j**-**l**, statistical significance was determined by two-tailed, unpaired Student's *t*-test, there is no significant difference between WT and *Susd2*$^{-/-}$ group ($P > 0.05$). All data are mean ± SD.

https://doi.org/10.1038/s41590-022-01326-8

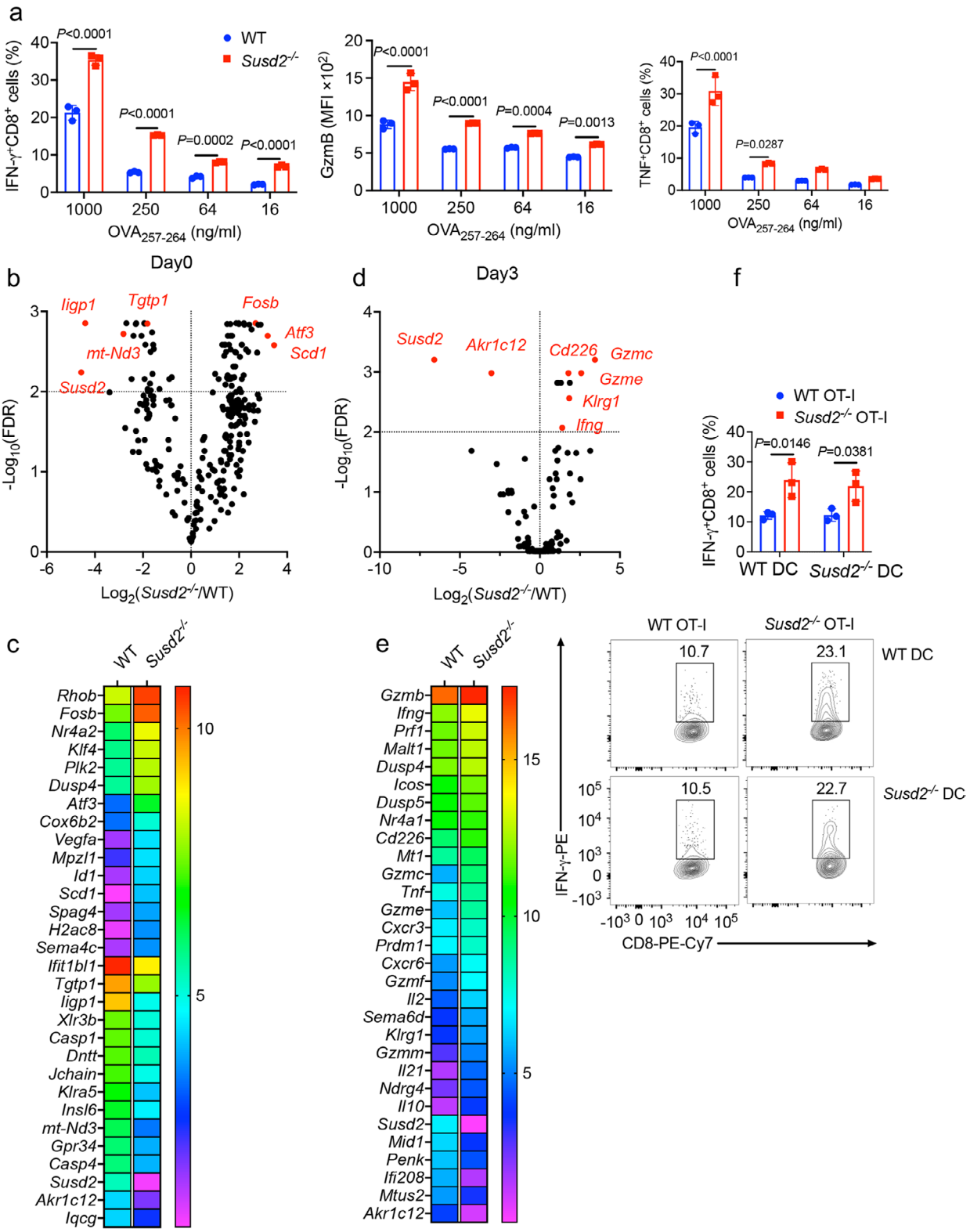

Extended Data Fig. 3 | *Susd2*$^{-/-}$ CD8$^+$ cells exhibit increased antitumor effector function. a, Flow cytometry analysis of IFN-γ$^+$CD8$^+$ T cells, GzmB$^+$CD8$^+$ T cells and TNF$^+$CD8$^+$ T cells in different $OVA_{257-264}$ dosage stimulated splenocytes isolated from WT or *Susd2*$^{-/-}$ OT-I mice. **b**-**e**, CD8$^+$ T cells were isolated from total splenocytes of either WT or *Susd2*$^{-/-}$ OT-I mice left untreated or stimulated with $OVA_{257-264}$ for 3 days and were subjected to RNA-seq assay. The volcano plot of RNA-seq data demonstrates differential gene expression between WT and *Susd2*$^{-/-}$ CD8$^+$ T cells at Day 0 (**b**) and Day 3 (**d**). A heat map of the top thirty genes representing genes differentially expressed between WT and *Susd2*$^{-/-}$ CD8$^+$ T cells at Day 0 (**c**) and Day 3 (**e**). **f**, Intracellular accumulation of IFN-γ in CD8$^+$ T cells isolated from WT or *Susd2*$^{-/-}$ OT-I mice that were co-cultured with either WT or *Susd2*$^{-/-}$ bone marrow-derived dendritic cells (BMDCs) that have been pulsed with $OVA_{257-264}$. **a**,**f**, $n = 3$, **b**-**e**, $n = 4$. *n*, number of mice per group. **a**,**f**, data are representative of four independent experiments. **b**-**e**, data are representative of two independent experiments. **b**,**d** statistical significance was calculated using two-sided Wilcoxon's rank-sum test and adjusted with Bonferroni's correction. Statistical significance was determined by two-way ANOVA followed by Sidak's multiple comparisons test(**a**,**f**) with *P* values noted in the figure. All data are mean ± SD.

https://doi.org/10.1038/s41590-022-01326-8

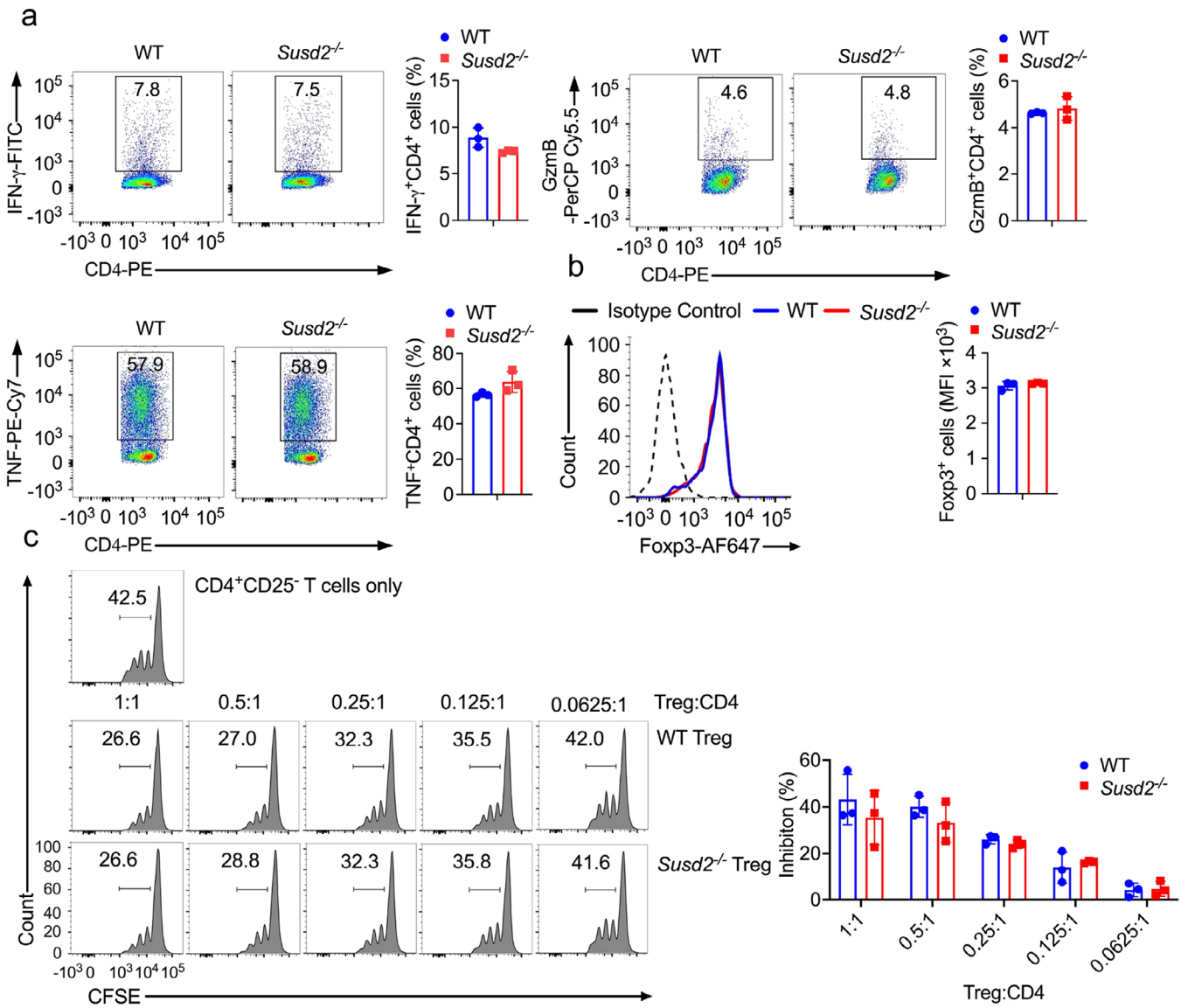

Extended Data Fig. 4 | *Susd2* deficiency does not affect effector function of CD4⁺ T cells or inhibitory function of Treg cells. a, Flow cytometry analysis of IFN-γ⁺CD4⁺ T cells, GzmB⁺CD4⁺ T cells and TNF⁺CD4⁺ T cells in $OVA_{323–339}$ stimulated splenocytes isolated from WT or *Susd2*$^{-/-}$ OT-II mice. **b**, Flow cytometry analysis of intranuclear level of Foxp3 in spleen CD4⁺ T cells from WT or *Susd2*$^{-/-}$ mice. **c**, Cell proliferation of naïve CD4⁺ T cells upon stimulation with CD3-CD28 antibody in the absence or presence of WT or *Susd2*$^{-/-}$ Treg cells at the indicated cell: cell ratio was measured by the staining of carboxyfluorescein diacetate succinimidyl ester (CFSE), followed by FACS analysis. **a**–**c**, $n = 3$. n, number of mice per group. Data are representative of four independent experiments. Statistical significance was determined by two-tailed, unpaired Student's t-test, there is no significant difference between WT and *Susd2*$^{-/-}$ group in **a**–**c** ($P > 0.05$). All data are mean ± SD.

https://doi.org/10.1038/s41590-022-01326-8

a

Human *IL2RA* sequencing:

CAATGGGAGCAATAGCAGAGCTCGTTTAGTGACCGTCAGAATTAACCATG**GACTACAAAGACCATGA**
CGGTGATTATAAAGATCATGACATCGATTACAAGGATGACGATGACAAGCTTGCGGCCGCGAATTCA
ATGGATTCATACCTGCTGATGTGGGGACTGCTCACGTTCATCATGGTGCCTGGCTGCCAGGCAGAGCT
CTGTGACGATGACCCGCCAGAGATCCCACACGCCACATTCAAAGCCATGGCCTACAAGGAAGGAACC
ATGTTGAACTGTGAATGCAAGAGAGGTTTCCGCAGAATAAAAAGCGGGTCACTCTATATGCTCTGTACA
GGAAACTCTAGCCACTCGTCCTGGGACAACCAATGTCAATGCACAAGCTCTGCCACTCGGAACACAAC
GAAACAAGTGACACCTCAACCTGAAGAACAGAAAGAAAGGAAAACCACAGAAATGCAAAGTCCAATGC
AGCCAGTGGACCAAGCGAGCCTTCCAGGTCACTGCAGGGAACCTCCACCATGGGAAAATGAAGCCAC
AGAGAGAATTTATCATTTCGTGGTGGGGCAGATGGTTTATTATCAGTGCGTCCAGGGATACAGGGCTC
TACACAGAGGTCCTGCTGAGAGCGTCTGCAAAATGACCCACGGGAAGACAAGGTGGACCCAGCCCCA
GCTCATATGCACAGGTGAAATGGAGACCAGTCAGTTTCCAGGTGAAGAGAAGCCTCAGGCAAGCCCC
GAAGGCCGTCCTGAGAGTGAGACTTCCTGCCTCGTCACAACAACAGATTTTCAAATACAGACAGAAAT
GGCTGCAACCATGGAGACGTCCATATTTACAACAGAGTACCAGGTAGCAGTGGCCGGCTGTGTTTTCC
TGCTGATCAGCGTCCTCCTCCTGAGTGGGCTCACCTGGCAGCGGAGACAGAGGAAGAGTAGAAGAAC
AATCTAGTCTAGAGGATCCCGGGTGGCATCCCTGTGACCCCTCCCCAGTGCCTCTCCTGGCCCTGGA
AGTTGCCACTCCAGTGCCCACCAGCCTTGTCCTAATAAAATTAAGTTGCATCATTTTGTCTGACTAGGT
GTCCTTCTATATATTATGGGGTGGAGGGGGGKGKGGWWWKGRRSCAAGGGGCAAGTTGGGAAGAMA
CCTGTAGGGCCTGCGGGTYTATTGGGAACCAAGCTGGAGTGCAGKGCACATCTGGCTCMCTGCATCT
CCGCCTCCTGGGTCAGCGATCTCCTGCCTCAGCCTCCCGAGTTGTGGGATTCAGGCATGCATGACAG
GCTCAGCTATTTTTGTTTTTTGTARRACGGTTTCACCATATTGGCAGCTGGTCTCCACTCCTATYYCAG
GKGATCTACCCACCTTGGCCTCCAAA

Underline: 3×Flag tag; ATG and TAG represent the start and stop codon, respectively.

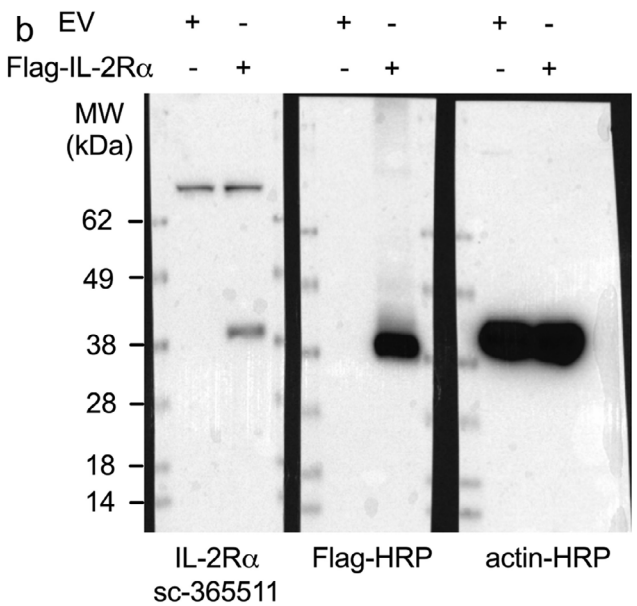

Extended Data Fig. 5 | The authenticity of the IL-2Rα molecular weight. a, Sanger sequencing result of pCMV3×Flag-IL2RA vector. **b**, Immunoblotting of Flag-IL2Rα in 293 T cells transfected with pCMV3×Flag-*IL2RA* vector. Data are representative of three independent experiments.

https://doi.org/10.1038/s41590-022-01326-8

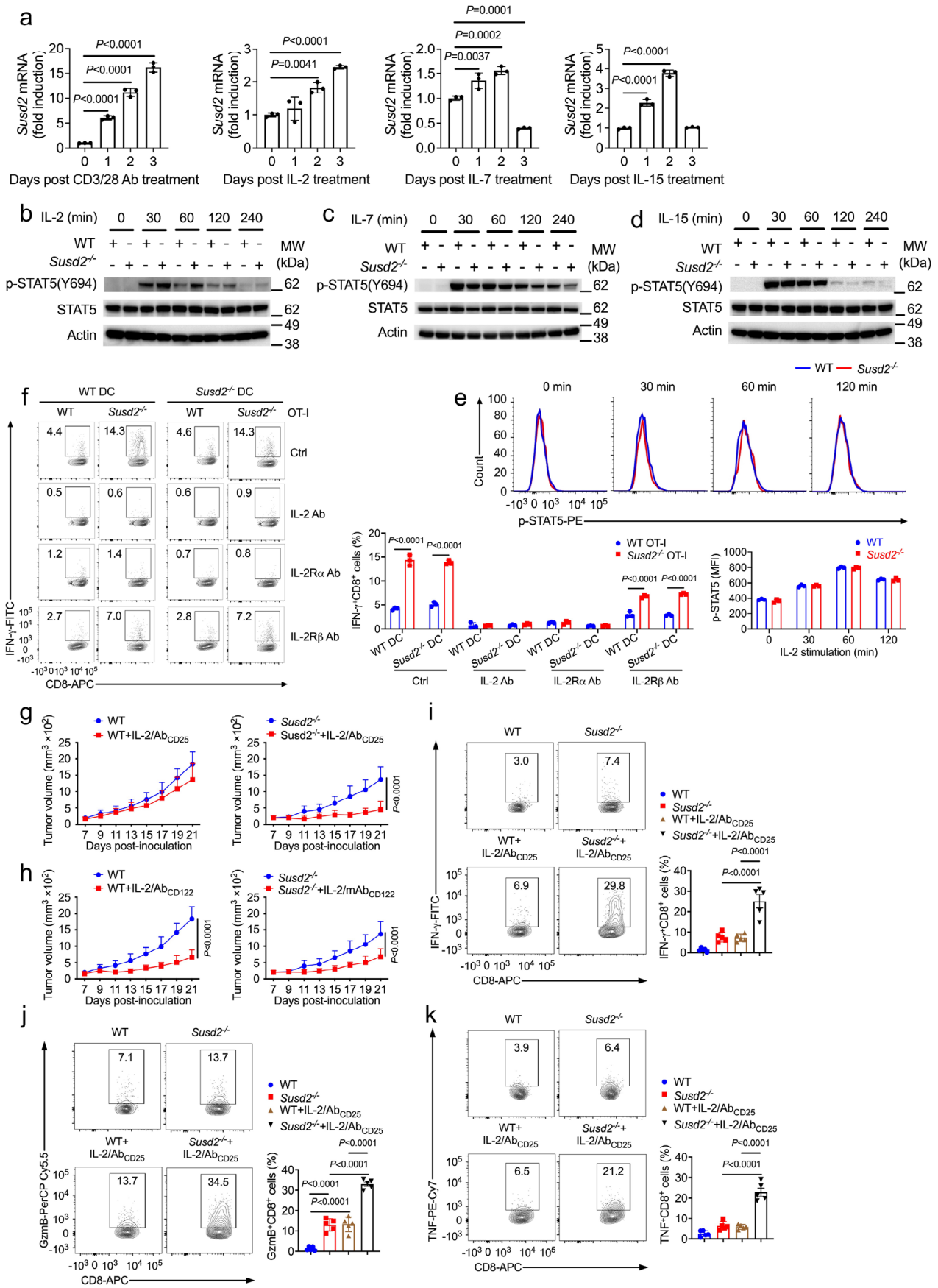

Extended Data Fig. 6 | See next page for caption.

https://doi.org/10.1038/s41590-022-01326-8

Extended Data Fig. 6 | Efficient control of tumor growth by IL-2/mAb$_{CD25}$ complex in *Susd2*$^{-/-}$ mice. a, Transcript of *Susd2* in mouse CD8$^+$ T cells stimulated with CD3-CD28 antibody, IL-2, IL-7 or IL-15 for 0, 1, 2 and 3 days. **b**-**d**, Immunoblotting of STAT5 in OVA$_{257-264}$-primed WT or *Susd2*$^{-/-}$ OT-I T cells which were rested overnight, and then stimulated with IL-2 (100 U/ml), IL-7 (5 ng/ml) or IL-15 (10 ng/ml) for 0, 30, 60, 120 and 240 minutes. **e**, Flow cytometry analysis of p-STAT5 in WT or *Susd2*$^{-/-}$ Treg cells stimulated with IL-2 (100 U/ml) for 0, 30, 60 and 120 minutes. **f**, CD8$^+$ T cells isolated from WT or *Susd2*$^{-/-}$ OT-I mice were co-cultured with WT or *Susd2*$^{-/-}$ bone marrow-derived dendritic cells (BMDCs) that have been pulsed with OVA$_{257-264}$. Intracellular accumulation of IFN-γ in WT or *Susd2*$^{-/-}$ CD8$^+$ T cells in the absence or presence of blocking antibodies against IL-2, IL-2Rα, or IL-2Rβ were measured by FACS analysis. **g**,**h**, Tumor growth in WT and *Susd2*$^{-/-}$ mice bearing B16-F10 tumor cells which were injected with IL-2/Ab$_{CD25}$ complex (**g**) or IL-2/Ab$_{CD122}$ complex(**h**). **i**-**k**, Flow cytometry analysis of intracellular accumulation of IFN-γ, GzmB and TNF-expressing intratumoral CD8$^+$ T cells. **a**,**e**,**f**, $n = 3$; **g**-**k**, $n = 5$. *n*, number of mice per group. **a**-**h**, data are representative of three independent experiments; **i**-**k**, data are representative of two independent experiments. Statistical significance was determined by two-way ANOVA followed by Sidak's multiple comparisons test (**e**-**g**) or one-way ANOVA followed by Tukey's test (**a**,**i**-**k**) with *P* values noted in the figure. All data are mean ± SD.

https://doi.org/10.1038/s41590-022-01326-8

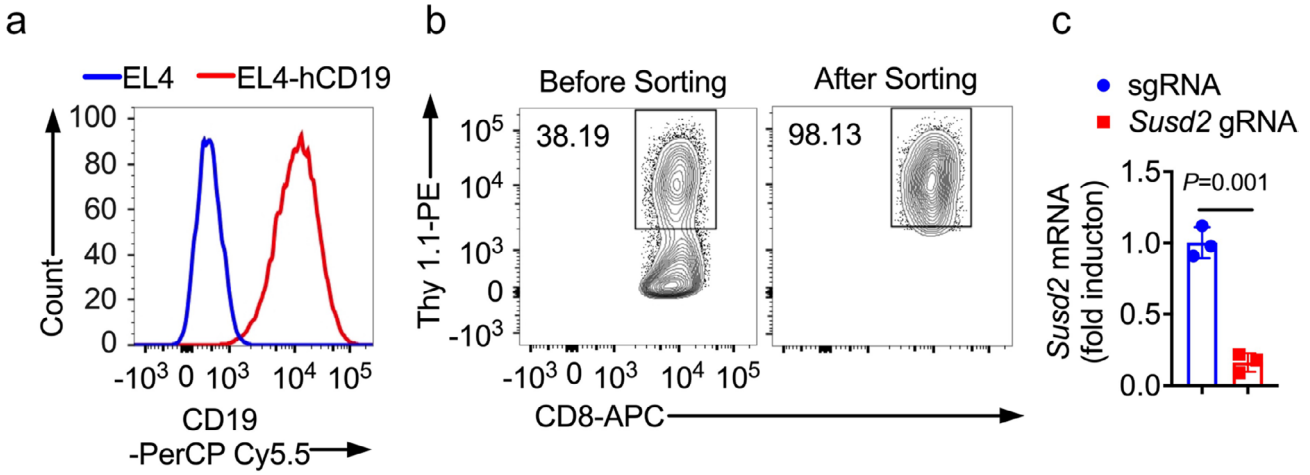

Extended Data Fig. 7 | Identification of EL4-hCD19 cells and CAR T cells. **a**, Validation of EL4 thymoma cell line expressing human CD19 (EL4-hCD19) with the deletion of its intracellular domain. **b**, Percentages of $CD8^+$ T cells retrovirally transduced with a chimeric antigen receptor (CAR) containing a portion of hCD19 single chain variable fragment (ScFv) fused with signaling domains of mouse CD28 and mouse CD3ζ sequence (with first and third ITAMs of the CD3ζ molecule inactivated) before and after cell sorting were assessed by the staining with anti-Thy1.1 antibody. **c**, Transcript of *Susd2* in CAR T cells that have been electroporated with scrambled gRNA(sgRNA) or Susd2 gRNA-Cas9 nucleoprotein (RNP) complex, sgRNA versus *Susd2* gRNA ($P = 0.0010$). **c**, $n = 3$. a–c, data are representative of two independent experiments. Statistical significance was determined by two-tailed, unpaired Student's *t*-test (**c**) with *P* values noted in the figure. The data represent mean ± SD.

https://doi.org/10.1038/s41590-022-01326-8

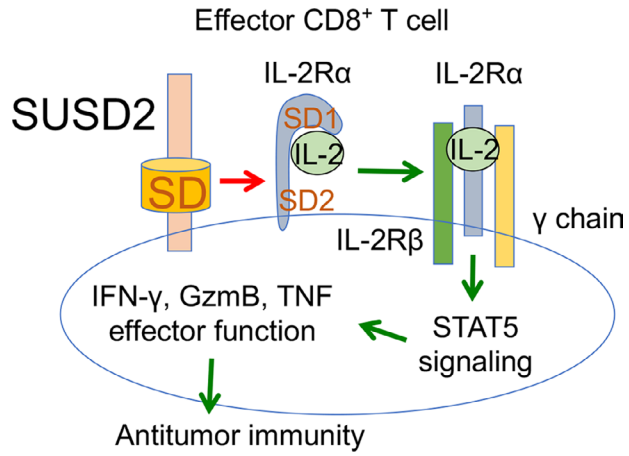

Extended Data Fig. 8 | A model for an inhibitory role of SUSD2 in effector CD8$^+$ T cell antitumor immunity by modulating IL-2R signaling. The present study has identified SUSD2 as a negative regulator of IL-2-mediated effector CD8$^+$ T cell functions and antitumor immunity. Both SUSD2 and IL-2Rα chain (IL-2Rα) contain the sushi domain (SD). Genetic ablation of SUSD2 (*Susd2*$^{-/-}$) leads to elevated IFN-γ, GzmB and TNF production in effector CD8$^+$ T cells and improved tumor growth control in multiple syngeneic tumor models. Mechanistically, SD-dependent interaction between SUSD2 and IL-2Rα competitively inhibits IL-2-IL-2Rα binding, leading to an attenuated IL-2R signaling. Therefore, SUSD2 represents a promising therapeutic target of tumor immunotherapy. Green and red arrows indicate promoting and inhibiting effect, respectively.

nature portfolio

Corresponding author(s): Haitao Wen

Last updated by author(s): Sep 3, 2022

Reporting Summary

Nature Portfolio wishes to improve the reproducibility of the work that we publish. This form provides structure for consistency and transparency in reporting. For further information on Nature Portfolio policies, see our Editorial Policies and the Editorial Policy Checklist.

Statistics

For all statistical analyses, confirm that the following items are present in the figure legend, table legend, main text, or Methods section.

n/a	Confirmed
☐	☒ The exact sample size (*n*) for each experimental group/condition, given as a discrete number and unit of measurement
☐	☒ A statement on whether measurements were taken from distinct samples or whether the same sample was measured repeatedly
☐	☒ The statistical test(s) used AND whether they are one- or two-sided *Only common tests should be described solely by name; describe more complex techniques in the Methods section.*
☒	☐ A description of all covariates tested
☒	☐ A description of any assumptions or corrections, such as tests of normality and adjustment for multiple comparisons
☐	☒ A full description of the statistical parameters including central tendency (e.g. means) or other basic estimates (e.g. regression coefficient) AND variation (e.g. standard deviation) or associated estimates of uncertainty (e.g. confidence intervals)
☒	☐ For null hypothesis testing, the test statistic (e.g. *F*, *t*, *r*) with confidence intervals, effect sizes, degrees of freedom and *P* value noted *Give P values as exact values whenever suitable.*
☒	☐ For Bayesian analysis, information on the choice of priors and Markov chain Monte Carlo settings
☒	☐ For hierarchical and complex designs, identification of the appropriate level for tests and full reporting of outcomes
☒	☐ Estimates of effect sizes (e.g. Cohen's *d*, Pearson's *r*), indicating how they were calculated

Our web collection on statistics for biologists contains articles on many of the points above.

Software and code

Policy information about availability of computer code

Data collection	Flow cytometry: BD FACSCanto™ II, Cytek® Aurora, BD FACSAria Fusion Cell Sorter, SONY MA900 Multi-Application Cell Sorter. Real-Time PCR: BIO-RAD CFX96 Touch™ Real-Time PCR Detection System. Mass Spectrometry: Thermo Fisher Scientific Orbitrap Eclipse Tribrid Mass Spectrometer. scRNA-seq: the NextSeq Illumina Platform. Bulk RNA-seq: NovaSeq 6,000 SP system (Illumina). Western Blotting: BIO-RAD ChemiDoc Imaging System.
Data analysis	Statistics and Data plotting: GraphPad Prism 8.0.1 Flow cytometry: FlowJo v 10.5.3, OMIQ data analysis software (www.omiq.ai) (Omiq), FlowSOM package Mass Spectrometry: MaxQuant-Andromeda software suite (version 1.6.3.4) scRNA-seq and Bulk RNA-seq: DESeq2 (v1.32.0)

For manuscripts utilizing custom algorithms or software that are central to the research but not yet described in published literature, software must be made available to editors and reviewers. We strongly encourage code deposition in a community repository (e.g. GitHub). See the Nature Portfolio guidelines for submitting code & software for further information.

Data

Policy information about availability of data

All manuscripts must include a data availability statement. This statement should provide the following information, where applicable:

- Accession codes, unique identifiers, or web links for publicly available datasets
- A description of any restrictions on data availability
- For clinical datasets or third party data, please ensure that the statement adheres to our policy

Data availability
ScRNA-seq and bulk RNA-seq data reported in this paper are accessible at the Gene Expression Omnibus under accessions GSE210704 and GSE212179, respectively. MS data have been deposited in an international public repository (MassIVE proteomics repository at https://massive.ucsd.edu/) under data set accession number MSV000087205. There are no restrictions for data availability. Source data are provided with this paper.

Field-specific reporting

Please select the one below that is the best fit for your research. If you are not sure, read the appropriate sections before making your selection.

☒ Life sciences ☐ Behavioural & social sciences ☐ Ecological, evolutionary & environmental sciences

For a reference copy of the document with all sections, see nature.com/documents/nr-reporting-summary-flat.pdf

Life sciences study design

All studies must disclose on these points even when the disclosure is negative.

Sample size	The sample size for each experiment is indicated in the figure legends. Sample sizes were based on our experience and common practice in the related fields, balancing statistic robustness, resource availability and animal welfare. For in vivo studies, 5-10 mice per group are sufficient to detect meaningful biological differences with good reproducibility. For in vitro studies, all the experiments were replicated at least for 3 individuals, independent experiments. No statistical methods were used to pre-determine sample sizes but our sample sizes are similar to those reported in previous publications (Nat Immunol. 2021;22(4):460-470., Nat Immunol. 2022;23(6):868-877. and Nat Immunol . 2022;23(3):386-398.).
Data exclusions	No data was excluded from this study.
Replication	Biological replicates are included to ensure the reproducibility and all repeated experiments are successful. Data reproducibility was confirmed by two-four independent experiments.
Randomization	Mice are sex- and age- matched and are randomly assigned to different treatment and control groups. In experiments not involving mice, we did not randomize because in vitro studies were observational and replicated at least for 3 individuals, independent experiments.
Blinding	For the establishment of initial observation in any tumor growth experiments, the measurement was conducted by a second personnel unaware of the information. No blinding was involved in other experiments, as machine-based readouts are not subject to investigator bias. Data collection and analysis were not performed blind to the conditions of the experiments.

Reporting for specific materials, systems and methods

We require information from authors about some types of materials, experimental systems and methods used in many studies. Here, indicate whether each material, system or method listed is relevant to your study. If you are not sure if a list item applies to your research, read the appropriate section before selecting a response.

Materials & experimental systems

n/a	Involved in the study
☐	☒ Antibodies
☐	☒ Eukaryotic cell lines
☒	☐ Palaeontology and archaeology
☐	☒ Animals and other organisms
☒	☐ Human research participants
☒	☐ Clinical data
☒	☐ Dual use research of concern

Methods

n/a	Involved in the study
☒	☐ ChIP-seq
☐	☒ Flow cytometry
☒	☐ MRI-based neuroimaging

Antibodies

Antibodies used	For flow cytometry analysis:

Antibodies used

Anti-mouse CD16/32 Antibody (Biolegend, Clone 93, Cat# 101302; RRID: AB_312801, 1:100 dilution),
Anti-mouse CD11b APC (Biolegend, Clone M1/70, Cat# 101212; RRID: AB_312795, 1:100 dilution),
Anti-mouse F4/80 FITC (Biolegend, Clone BM8, Cat# 123108, RRID: AB_893502, 1:100 dilution),
Anti-mouse CD11c PE-Cy5 (Biolegend, Clone N418, Cat# 117316, RRID: AB_493566, 1:100 dilution),
Anti-mouse Ly6C PE, Biolegend, Clone HK1.4, Cat# 128008, RRID: AB_1186132, 1:100 dilution),
Anti-mouse Ly6G Pacific Blue (Biolegend, Clone 1A8, Cat# 127612, RRID: AB_2251161, 1:100 dilution),
Anti-mouse CD3 FITC (Biolegend, Clone 145-2C11, Cat# 100306, RRID: AB_312671, 1:100 dilution),
Anti-mouse CD4 PE (Biolegend, Clone GK1.5, Cat# 100408, RRID: AB_312693, 1:100 dilution),
Anti-mouse CD8 APC (Biolegend, Clone 53-6.7, Cat# 100712, RRID: AB_312751, 1:100 dilution),
Anti-mouse CD8 PE-Cy7 (Biolegend, Clone 53-6.7, Cat# 100722, RRID: AB_312761, 1:100 dilution),
Anti-mouse CD25 PE-Cy5 (Biolegend, Clone PC61, Cat# 102010, RRID: AB_312859, 1:100 dilution),
Anti-mouse Foxp3 Alexa Fluor 647 (Biolegend, Clone MF-14, Cat# 126408, RRID: AB_1089115, 1:100 dilution),
Anti-mouse IFN-γ FITC (Biolegend, Clone XMG1.2, Cat# 505806, RRID: AB_315400, 1:100 dilution),
Anti-mouse IFN-γ PE (Biolegend, Clone XMG1.2, Cat# 505808, RRID: AB_315402, 1:100 dilution),
Anti-mouse TNF-α APC (Biolegend, Clone MP6-XT22, Cat# 506308, RRID: AB_315429, 1:100 dilution),
Anti-mouse TNF-α PE-Cy7 (Biolegend, Clone MP6-XT22, Cat# 506324, RRID: AB_2256076, 1:100 dilution),
Anti-mouse GzmB PerCP Cy5.5 (Biolegend, Clone QA16A02, Cat# 372212, RRID: AB_2728379, 1:100 dilution),
Anti-mouse GzmB PE (eBioscience, Clone NGZB, Cat# 12-8898-82, RRID: AB_10870787, 1:100 dilution),
Anti-mouse CD90.1(Thy-1.1) PE (Biolegend, Clone OX-7, Cat# 202524, RRID: AB_1595524, 1:100 dilution),
Anti-mouse CD90.2(Thy-1.2) Pacific Blue (Biolegend, Clone 53-2.1, Cat# 140306, RRID: AB_10641693, 1:100 dilution),
Anti-mouse NK1.1 Pacific Blue (Biolegend, Clone PK136, Cat# 108722, RRID: AB_2132712, 1:100 dilution),
Anti-mouse CD19 Pacific Blue (Biolegend, Clone 6D5, Cat# 115523, RRID: AB_439718, 1:100 dilution),
Anti-mouse CD19 APC (Biolegend, Clone 6D5, Cat# 115512, RRID: AB_313647, 1:100 dilution),
Anti-mouse PD-1 PE-Cy7 (Biolegend, Clone 29F.1A12, Cat# 135216, RRID: AB_10689635, 1:100 dilution),
Anti-mouse LAG3 PerCP Cy5.5 (Biolegend, Clone C9B7W, Cat# 125212, RRID: AB_2561517, 1:100 dilution),
PE Mouse Anti-Stat5 (pY694) (BD Biosciences, Clone 47/Stat5(pY694), Cat# 612567, RRID: AB_399858, 1:100 dilution),
Anti-human CD8 Antibody (APC, Biolegend, Clone HIT8a, Cat# 300912, RRID: AB_314116, 1:100 dilution),
Anti-human CD4 Antibody FITC, (Biolegend, Clone OKT4, Cat# 317408, RRID: AB_571951, 1:100 dilution),
Anti-human CD14 Antibody PE (Biolegend, Clone M5E2, Cat# 301806, RRID: AB_314188, 1:100 dilution),
Anti-human CD19 Antibody Pacific Blue (Biolegend, Clone HIB19, Cat# 302224, RRID: AB_493653, 1:100 dilution),
TCF1/TCF7 (C63D9) Rabbit mAb (Alexa Fluor® 488 Conjugate) (Cell Signaling Technology, Clone C63D9, Cat#6444, 1:100 dilution),
TCF1/TCF7 (C63D9) Rabbit mAb (PE Conjugate) (Cell Signaling Technology, Clone C63D9, Cat#14456, 1:100 dilution),
PE anti-mouse IL-2 Antibody (Biolegend, Clone JES6-5H4, Cat# 503808, RRID: AB_315302, 1:100 dilution).
LIVE/DEAD™ Fixable Blue Dead Cell Stain Kit, for UV excitation (Invitrogen, Cat# L34962A, 1:100 dilution),
Brilliant Violet 510™ anti-mouse CD45 Antibody (Biolegend, Clone 30-F11, Cat# 103138, RRID: AB_2563061, 1:100 dilution),
BUV737 Hamster Anti-Mouse CD3e (BD Horizon™, Clone 145-2C11, Cat# 612771, RRID: AB_2870100, 1:100 dilution),
BUV496 Rat Anti-Mouse CD8a (BD OptiBuild™, Clone 53-6.7, Cat# 750024, RRID: AB_2874242, 1:100 dilution),
CD4 Monoclonal Antibody PerCP-Cyanine5.5 (eBioscience™, Clone RMF-5, Cat# 45-0042-82, RRID: AB_1107001, 1:100 dilution),
CD11b Monoclonal Antibody Alexa Fluor 532(eBioscience™, Clone M1/70, Cat# 58-0112-82, RRID: AB_2811905, 1:100 dilution),
Brilliant Violet 570™ anti-mouse NK-1.1 Antibody (Biolegend, Clone PK136, Cat# 108733, RRID: AB_10896952, 1:100 dilution),
FOXP3 Monoclonal Antibody eFluor 450 (eBioscience™, Clone FJK-16s, Cat# 48-5773-82, RRID: AB_1518812, 1:100 dilution),
Brilliant Violet 711™ anti-mouse CD366 (Tim-3) Antibody (Biolegend, Clone RMT3-23, Cat# 119727, RRID: AB_2716208, 1:100 dilution),
CD279 (PD-1) Monoclonal Antibody FITC, (eBioscience™, Clone J43, Cat# 11-9985-82, RRID: AB_465472, 1:100 dilution),
BB515 Rat Anti-Mouse CD25 (BD Horizon™, Clone PC61, Cat# 564424, RRID: AB_2738803, 1:100 dilution),
Brilliant Violet 421™ anti-mouse CD62L Antibody (Biolegend, Clone MEL-14, Cat# 104436, RRID: AB_2562560, 1:100 dilution),
PE/Cyanine5 anti-mouse CD69 Antibody (Biolegend, Clone H1.2F3, Cat# 104510, RRID: AB_313113, 1:100 dilution),
BUV661 Rat Anti-Mouse CD44 (BD OptiBuild™, Clone IM7, Cat# 741471, RRID: AB_2870939, 1:100 dilution),
BUV805 Rat Anti-Mouse CD223(Lag3) (BD OptiBuild™, Clone C9B7W, Cat# 748540, RRID: AB_2872950, 1:100 dilution),
VISTA Monoclonal Antibody Super Bright 600 (eBioscience™, Clone MIH64 Cat# 63-1083-82, RRID: AB_2725663, 1:100 dilution),
BV650 Mouse Anti-Mouse TIGIT (BD OptiBuild™, Clone 1G9, Cat# 744213, RRID: AB_2742062, 1:100 dilution),
BUV563 Hamster Anti-Mouse CD27 (BD OptiBuild™, Clone LG.3A10, Cat# 741275, RRID: AB_2870816, 1:100 dilution),
BV750 Rat Anti-Mouse CD38 (BD OptiBuild™, Clone 90/CD38, Cat# 747103, RRID: AB_2871855, 1:100 dilution),
KLRG1 Monoclonal Antibody Pacific Orange (eBioscience™, Clone 2F1, Cat# 79-5893-82, RRID: AB_2815359, 1:100 dilution),
CD278 (ICOS) Monoclonal Antibody Super Bright 436 (eBioscience™, Clone C39B.4A, Cat# 62-9949-82, RRID: AB_2744820, 1:100 dilution),
BV480 Hamster Anti-Mouse CD95 (Fas) (BD OptiBuild™, Clone Jo2, Cat# 746755, RRID: AB_2744016, 1:100 dilution),
BUV615 Hamster Anti-Mouse CD103 (BD OptiBuild™, Clone 2E7, Cat# 751631, RRID: AB_2875624, 1:100 dilution),
APC/Fire™ 750 anti-mouse CD183 (CXCR3) Antibody (Biolegend, Clone CXCR3-173, Cat# 126539, RRID: AB_2650829, 1:100 dilution),
PE/Dazzle™ 594 anti-mouse CD39 Antibody (Biolegend, Clone Duha59, Cat# 143812, RRID: AB_2750322, 1:100 dilution),
TOX Antibody, anti-human/mouse PE (Miltenyi Biotec, Clone REA473, Cat# 130-120-716, RRID: AB_2751485, 1:100 dilution),
TCF1/TCF7 (C63D9) Rabbit mAb (PE-Cy7® Conjugate) (Cell Signaling Technology, Clone C63D9, Cat# 90511, 1:100 dilution),
BUV395 Mouse Anti-Ki-67 (BD OptiBuild™, Clone B56, Cat# 564071, RRID: AB_2738577, 1:100 dilution),
EOMES Monoclonal Antibody PerCP-eFluor 710 (eBioscience™, Clone Dan11mag, Cat# 46-4875-82, RRID: AB_10597455, 1:100 dilution),
BV786 Rat Anti-Mouse IFN-γ (BD Horizon™, Clone XMG1.2, Cat# 563773, RRID: AB_2738419, 1:100 dilution),
APC anti-mouse TNF-α Antibody (Biolegend, Clone MP6-XT22, Cat# 506308, RRID: AB_315428, 1:100 dilution),
Alexa Fluor® 700 anti-human/mouse Granzyme B Recombinant Antibody (Biolegend, Clone QA16A02, Cat# 372222, RRID: AB_2728389, 1:100 dilution).

For T cell stimulation:
Anti-mouse CD3 Antibody (Biolegend, Clone 17A2, Cat# 100238, RRID: AB_2561487),
Anti-mouse CD28 Antibody (Biolegend, Clone 37.51, Cat# 102116, RRID: AB_11147170), Anti-human CD3 Antibody (Biolegend, Clone UCHT1, Cat# 300438, RRID: AB_11146991), Anti-human CD28 Antibody (Biolegend, Clone CD28.2, Cat# 302934, RRID: AB_11148949).

For immunoblotting:
Anti-SUSD1 antibody (Sigma-Aldrich, Cat# HPA048554, 1:1000)
Anti-SUSD2 antibody (Sigma-Aldrich, Cat# HPA004117, 1:1000),
Phospho-Stat5 (Tyr694) Antibody (Cell Signaling Technology, Cat# 9351, 1:1000),
Stat5 Antibody (Cell Signaling Technology, Cat# 9363, 1:1000),
Mouse CD25/IL-2R alpha Antibody, (R&D, Cat# AF2438-SP, 1:1000),
Anti-IL-2Rα Antibody (C-11) (Santa Cruz, Cat# sc-365511, 1:1000),
Anti-IL-2Rβ Antibody (C-10) (Santa Cruz, Cat# sc-393093, 1:1000),
Recombinant Anti-IL-2RG antibody (abcam, Cat# ab273023, 1:1000),
anti-IL-15Rα Antibody (G-3) (Santa Cruz, Cat# sc-374023, 1:1000)
anti-Mucin 4 Antibody (1G8) (Santa Cruz, Cat# sc-33654, 1:1000)
V5 Tag Antibody (Thermo, Cat# R960-25, 1:1000),
Anti-Myc Tag Antibody, HRP conjugate (clone 4A6) (Sigma-Aldrich, Cat# 16-213, 1:1000),
Flag-HRP mAb (Genscript, Clone, 5A8E5 Cat# A01428, 1:2000),
Anti-Actin (Santa Cruz, Cat# sc-1615, 1:1000),
Anti-mouse IgG, HRP-linked Antibody (Cell Signaling Technology, Cat#7076, 1:3000),
Anti-rabbit IgG, HRP-linked Antibody (Cell Signaling Technology, Cat#7074, 1:3000).

For the in vitro experiments:
Anti-mouse IL-2 Antibody (Biolegend, Clone JES6-1A12, Cat# 503706, RRID: AB_11150775, 10 µg/ml),
Anti-mouse CD25 (IL-2Rα) Antibody (Biolegend, Clone PC61, Cat# 102040, RRID: AB_11150394, 10 µg/ml),
Anti-mouse CD122 (IL-2Rβ) Antibody (Biolegend, Clone TM-β1, Cat# 123224, RRID: AB_2810373, 10 µg/ml).

For the in vivo experiments:
InVivo MAb anti-mouse CD8α (BioXcell, Clone YTS 2.43, Cat# BE0061, RRID: AB_10950145),
InVivo MAb anti-mouse PD-L1 (B7-H1) (BioXcell, Clone 10F.9G2, Cat# BE0101, RRID: AB_10949073),
InVivo MAb rat IgG2b isotype control (BioXcell, Clone LTF-2, Cat# BE0090, RRID: AB_1107780),
InVivo MAb anti-mouse PD-1 (CD279) (BioXcell, Clone RMP1-14, Cat# BE0146, RRID: AB_10949053),
InVivo MAb rat IgG2a isotype control (BioXcell, Clone 2A3, Cat# BE0089, RRID: AB_1107769),
InVivo MAb anti-mouse IL-2 (BioXcell, Clone JES6-1A12, Cat# BE0043, RRID: AB_1107702),
InVivoMAb anti-mouse IL-2 (BioXcell, Clone S4B6-1, Cat# BE0043-1).

Validation

All antibodies were well-recognized clones in the field, commercially available and validated by the manufacturers. The information about host specificity, reactivity and applications are freely available on the vendors web under the indicated catalog number of each antibody, or easily get from website (https://scicrunch.org/resources/data/source/nif-0000-07730-1/search) by Research Resource Identifiers (#RRID) number.

Eukaryotic cell lines

Policy information about cell lines

Cell line source(s)

Human 293T cell line (CRL-3216), B16-F10 cell line (murine melanoma, CRL-6475), EL4 cell line (murine thymoma, TIB39), EG7 cell line (murine thymoma expressing OVA, CRL-2113), Jurkat cell line (clone E6-1, TIB152) and Phoenix Eco Packaging cell line (CRL-3214) were purchased from the American Type Culture Collection (ATCC). B16-OVA cell line (SCC420) was purchased for Sigma-Aldrich. MC38 cell line (murine colon adenocarcinoma, RRID: CVCL_B288) was purchased from the American Type Culture Collection (ATCC) and kindly provided by Dr. Yangxin Fu (UT Southwestern Medical Center). Platinum-E (Plat-E) Retroviral Packaging cell Line (RV-101) was purchased from Cell Biolabs.

Authentication

None of the cell lines were independently authenticated.

Mycoplasma contamination

All cell lines were tested for mycoplasma contamination and were not contaminated.

Commonly misidentified lines
(See ICLAC register)

No commonly misidentified cell lines were used.

Animals and other organisms

Policy information about studies involving animals; ARRIVE guidelines recommended for reporting animal research

Laboratory animals

All mice were housed in the specific pathogen-free facility and all in vivo experiments were performed in according with the guidelines established by The Ohio State University and National Institute of Health Guide for the Care and Use of Laboratory Animals and the Institutional Animal Care and Use Committee (IACUC). Susd2−/− mice were generated by Cyagen Biosciences with a CRISPR/Cas9-mediated genome engineering strategy. C57BL/6J mice (000664), Thy1.1 mice (000406), Rag2−/− mice (008449) and OT-I mice (003831) were obtained from the Jackson Laboratory. OT-II mice have been previously described (Wen, H., Lei, Y., Eun, S.Y. & Ting, J.P., J Exp Med, 2010, 207, 2943-2957). Susd2−/− OT-I and Susd2−/− OT-II mice were generated by crossing Susd2−/− with OT-I and OT-II mice, respectively. Eight to ten-week-old, female and male mice were used.

Wild animals

No wild animals were used in the study.

Field-collected samples

No field-collected samples were employed in this study.

Ethics oversight	All mice were housed in SPF facilities and all in vivo experiments were conducted in accordance with the National Institute of Health Guide for the Care and Use of Laboratory Animals and the Institutional Animal Care and Use Committee (IACUC). The study was approved by The Ohio State University and National Institute of Health Guide for the Care and Use of Laboratory Animals and the Institutional Animal Care and Use Committee (IACUC) (Protocol: 2018A00000022-R1) and all procedures were conducted in accordance with the experimental animal guidelines of The Ohio State University .

Note that full information on the approval of the study protocol must also be provided in the manuscript.

Flow Cytometry

Plots

Confirm that:

☒ The axis labels state the marker and fluorochrome used (e.g. CD4-FITC).

☒ The axis scales are clearly visible. Include numbers along axes only for bottom left plot of group (a 'group' is an analysis of identical markers).

☒ All plots are contour plots with outliers or pseudocolor plots.

☒ A numerical value for number of cells or percentage (with statistics) is provided.

Methodology

Sample preparation	Mouse spleens were passed through 70-µm cell strainers. Spleen cell suspensions were lysed with ACK lysis buffer. Tumors were minced into small fragments and digested with 1 mg/mL collagenase IV and 50 U/mL DNase I for 30 min at 37°C. Samples were mechanically disaggregated and filtered with 70-µm cell strainers. Single cell suspensions were treated with purified anti-CD16/32 (Fc receptor block, clone 93; BioLegend), and then stained with fluorochrome-conjugated monoclonal antibodies (clones mentioned in parentheses).
Instrument	BD FACSCanto™ II, Cytek® Aurora, BD FACSAria Fusion Cell Sorter and SONY MA900 Multi-Application Cell Sorter were used for flow cytometry data collection.
Software	FlowJo v 10.5.3 was used for flow cytometric data analysis.
Cell population abundance	Cell populations were sorted to >95% purity as determined by flow cytometry.
Gating strategy	Cells were identified with FSC-A/SSC-A gating and followed by FSC-H/FSC-A for singlets. All gates were set based on FMO (full-minus one) stains and isotype control antibodies after appropriate compensation using single-stained compensation controls.

☐ Tick this box to confirm that a figure exemplifying the gating strategy is provided in the Supplementary Information.